

# Block-coordinate Plug-And-Play Methods with Armijo-like line-search for Image Restoration\*

F. Porta<sup>†</sup>      S. Rebegoldi<sup>†</sup>      A. Sebastiani<sup>†</sup>

March 3, 2026

## Abstract

In this paper, we develop a class of block-coordinate Plug-and-Play (PnP) methods to address imaging inverse problems. The block-coordinate strategy is designed to reduce the high memory consumption arising in PnP methods that rely on Gradient Step denoisers, whose implementation typically requires storing large computational graphs. The proposed methods are based on a block-coordinate forward-backward framework for solving non-convex and non-separable composite optimization problems. Furthermore, such methods allow for the joint use of inertial acceleration, variable metric strategies, inexact proximal computations, and adaptive steplength selection via an appropriate line-search procedure. Under mild assumptions on the objective function, we establish a sublinear convergence rate and the stationarity of the limit points. Moreover, convergence of the entire sequence of the iterates is guaranteed under a Kurdyka-Łojasiewicz assumption. Numerical experiments on ill-posed imaging problems, including deblurring and super-resolution, demonstrate that the proposed PnP approach achieves state-of-the-art reconstruction quality while substantially reducing GPU memory requirements, making it particularly suitable for large-scale and resource-constrained imaging applications.

## 1 Introduction

The main goal of imaging inverse problems is to recover an unknown image  $x \in \mathbb{R}^n$  from measurements  $b \in \mathbb{R}^m$ , which are related through a linear acquisition model  $b = Ax + \eta$ , where  $A \in \mathbb{R}^{m \times n}$  is the forward operator, mapping the image space to the measurement space, and  $\eta \in \mathbb{R}^m$  denotes additive measurement noise. Since such inverse problems are typically ill-posed, direct inversion does not provide meaningful solutions.

Variational approaches to image restoration [7, 44] propose to recover an approximation of the unknown image as the solution of an optimization problem of the form

$$\operatorname{argmin}_{x \in \mathbb{R}^n} F(x) \equiv \phi(x) + f(x), \quad (1)$$

where  $\phi : \mathbb{R}^n \rightarrow \mathbb{R}$  is a data fidelity term, typically related to the noise distribution and measuring the likelihood of the observed data given the unknown image, and  $f : \mathbb{R}^n \rightarrow \mathbb{R}$  is a regularization term, enforcing stability and a priori information on the solution. The explicit choice of the second term usually depends on prior knowledge of the image; however, arbitrary assumptions may introduce bias or artifacts, such as the staircasing effect associated with the Total Variation regularization.

Plug-and-Play (PnP) approaches [43] represent a powerful and innovative paradigm for solving inverse problems in computational imaging by replacing the usual explicit regularization step with an implicit step, implemented by means of a denoising algorithm. This makes the PnP approach very

---

\*Submitted to the editors 28/02/2026.

<sup>†</sup>Dipartimento di Scienze Fisiche, Informatiche e Matematiche, Università di Modena e Reggio Emilia, Via Campi 213/b, 41125 Modena, Italy

modular and flexible, since any off-the-shelf denoiser can be plugged into the framework. Instead of designing a hand-crafted regularization term, cutting-edge denoisers can be embedded into the algorithm, often outperforming traditional regularization techniques. Indeed, in the last decade, PnP methods have achieved state-of-the-art results in several image restoration tasks [2, 15, 32, 48, 49]. Despite having demonstrated remarkable empirical performance, the convergence properties of PnP algorithms often rely on restrictive assumptions, including strong convexity of the data-fidelity term [40] and constraints on the denoiser, such as near-non-expansiveness or symmetric Jacobians, that may degrade performance [35, 38, 39, 40, 45].

In order to address these convergence issues, recent works have focused on designing denoisers with a clearer variational interpretation. In [29] a new denoising operator has been proposed, defined explicitly as the gradient step of a potential function parametrized by a convolutional neural network. More precisely, given a noise level  $\sigma \in \mathbb{R}^+$  and a smooth function  $g_\sigma : \mathbb{R}^n \rightarrow \mathbb{R}$ , the Gradient Step (GS) denoiser is defined as

$$D_\sigma(x) = x - \nabla g_\sigma(x). \quad (2)$$

In practice, the authors in [29] propose to choose

$$g_\sigma(x) = \frac{1}{2} \|x - N_\sigma(x)\|^2, \quad (3)$$

where  $N_\sigma : \mathbb{R}^n \rightarrow \mathbb{R}^n$  is any differentiable neural network architecture that has proven to be efficient for image denoising. In this framework, given a positive regularization parameter  $\lambda$ , the term  $f$  in (1) takes the form  $\lambda g_\sigma$  and, by following [29], the resulting optimization problem is solved by means of a PnP method whose general iteration can be seen as a forward-backward step on (1), i.e.,

$$x_{k+1} = \text{prox}_{\alpha\phi}(x_k - \alpha\nabla f(x_k)) = \text{prox}_{\alpha\phi}(x_k - \alpha\lambda\nabla g_\sigma(x_k)), \quad (4)$$

where  $\alpha \in \mathbb{R}^+$  is a suitable steplength and  $\text{prox}_{\alpha\phi}$  denotes the proximal operator of  $\alpha\phi(\cdot)$ , namely

$$\text{prox}_{\alpha\phi}(x) = \underset{y \in \mathbb{R}^n}{\text{argmin}} \frac{1}{2} \|y - x\|^2 + \alpha\phi(y), \quad \forall x \in \mathbb{R}^n. \quad (5)$$

Remarkably, by leveraging convergence results valid for the standard forward-backward method in the non-convex setting, in [29] the authors deduce that the PnP scheme (4) converges to a stationary point of  $\phi + \lambda g_\sigma$ , even when the data-fidelity term is not strongly convex and without assuming the non-expansiveness of the denoiser. The main limitation of the PnP forward-backward approach in (4) is the evaluation of  $\nabla g_\sigma$ . Indeed, in view of (2) and the definition of  $g_\sigma$  in (3), the gradient of  $g_\sigma$  can be written explicitly as

$$\nabla g_\sigma(x) = x - D_\sigma(x) = x - N_\sigma(x) - J_{N_\sigma}(x)^T(x - N_\sigma(x)), \quad (6)$$

where  $J_{N_\sigma}(x)$  denotes the Jacobian of  $N_\sigma$  evaluated at  $x$ , which can be computed via an automatic differentiation pipeline. As a consequence, the forward step in (4) requires the computation of the Jacobian  $J_{N_\sigma}(x)$  using a backpropagation routine that stores the entire computational graph associated to the neural network. Unfortunately, the memory required for this operation scales with the image size, which significantly limits the applicability of GS denoisers and the corresponding PnP algorithm (4) on real applications in resource-constrained settings.

*Contributions.* The contribution of this work is twofold. On the one hand, a block-coordinate forward-backward framework for solving (1) is proposed; on the other hand, such a framework is leveraged to define a novel class of block-coordinate PnP methods based on a GS denoiser of the form (2)-(3). The block-coordinate strategy is aimed at efficiently reducing the memory-consumption due to the computation of the GS denoiser. More precisely, we propose a general block-coordinate forward-backward framework that does not require the objective function in problem (1) to be separable. Allowing both terms in (1) to be potentially non-separable enables the proposed approach to address

minimization problems where  $\phi$  is a non-separable data-fidelity term and  $f = \lambda g_\sigma$ , with  $\lambda \in \mathbb{R}^+$  and  $g_\sigma$  defined in (3). The proposed framework is analyzed under the assumption that  $f : \mathbb{R}^n \rightarrow \mathbb{R}$  has a Lipschitz continuous gradient, and  $\phi : \mathbb{R}^n \rightarrow \mathbb{R}$  is continuously differentiable with a locally Lipschitz continuous gradient and convex along the coordinates. Classical data fidelity terms, as well as the previously introduced function  $g_\sigma$ , satisfy these assumptions. The proposed block-coordinate structure is then applied with  $f = \lambda g_\sigma$ , considering the patches of the image as the blocks of coordinates and employing a proper and efficient computation of  $\nabla g_\sigma$  on each block, which can be derived by exploiting the properties of convolutional neural networks.

The proposed block-coordinate forward-backward framework can be considered as a generalization of the Proximal Heavy-ball Inexact Line-search Algorithm (PHILA) devised in [13] to the alternating block-coordinate setting. The PHILA method applied to problem (1) relies on the following iteration

$$\begin{aligned} \tilde{y}_k &\approx \text{prox}_{\alpha_k \phi}^{D_k} (x_k - \alpha_k D_k^{-1} \nabla f(x_k) + \beta_k (x_k - x_{k-1})) \\ x_{k+1} &= x_k + \lambda_k (\tilde{y}_k - x_k), \end{aligned} \quad (7)$$

where  $\alpha_k$  and  $\beta_k$  are positive parameters,  $D_k$  is a symmetric and positive definite matrix,  $\text{prox}_{\alpha_k \phi}^{D_k}(\cdot)$  is the proximal operator of  $\alpha_k \phi$  with respect to the norm induced by  $D_k$ , and  $\lambda_k \in (0, 1]$  is selected by an Armijo-like line-search procedure, to guarantee a sufficient decrease of a proper merit function. The inexact computation of the proximal operator related to the data fidelity term  $\phi$  is also allowed. Extending PHILA to a block-coordinate framework requires a careful design of the inertial terms across blocks, together with the definition of a suitable merit function decreasing throughout the iterations. Under the previously stated assumptions on the functions  $\phi$  and  $f$ , we prove a sublinear convergence rate and the stationarity of the limit points. Furthermore, if appropriate surrogate functions of  $F$  satisfy the Kurdyka-Łojasiewicz property on their domains, convergence of the entire sequence generated by the proposed framework and related convergence rates on the function values can be established. Numerical experiments on ill-posed imaging problems, such as deblurring and super-resolution, show that the block-coordinate PHILA approach achieves state-of-the-art image restoration performance while significantly reducing GPU memory usage. This property makes the proposed framework particularly suitable for resource-constrained environments and large-scale imaging problems.

The reader may wonder why a forward-backward approach is adopted to solve (1), rather than a full gradient scheme, even though both terms  $\phi$  and  $f$  are assumed to be differentiable. This choice can be justified by several considerations. (i) As shown in [20], activating smooth functions through their gradients and nonsmooth ones through their proximity operators is not necessarily the most efficient strategy from a numerical standpoint, since proximal steps may positively affect the asymptotic performance of algorithms, particularly in image restoration problems. (ii) The Lipschitz constant of  $\nabla \phi + \nabla f$  may be significantly larger than that of  $\nabla f$  [6, Section 9.3], which leads to smaller feasible steplengths for the full gradient method, due to the inverse dependence on the Lipschitz constant of  $\nabla \phi + \nabla f$ . (iii) Finally, the approach proposed in [29], which inspired this work and relies on the forward-backward iteration (4), has demonstrated strong empirical performance across various imaging tasks. Our numerical experiments further confirm that a forward-backward strategy seems preferable to a full gradient approach when solving imaging problems with PnP schemes.

*Related works.* We remark that several block-coordinate forward-backward methods for possibly non-convex optimization have already been proposed in the literature, often incorporating either inertial acceleration or variable metric strategies [12, 19, 22, 25, 34, 36, 37, 46, 47]. However, these approaches typically do not combine both mechanisms and are tailored to problems of the form (1) with separable (possibly non-smooth) regularization terms, which limits their applicability to settings involving differentiable but non-separable objectives, such as PnP frameworks. While a few methods address non-separable composite problems [1, 18, 24, 26, 30, 33], they generally rely on restrictive steplength rules, lack line-search strategies, do not allow inexact proximal computations, and do not exploit inertial or variable metric acceleration. In contrast, the approach proposed in this paper is specifically designed for non-convex and non-separable problems, offering provable convergence guarantees together with adaptive step-size selection and the joint use of inertial and variable metric

strategies.

To the best of our knowledge, only a very limited number of works on block-coordinate PnP algorithms exist in the literature [23, 28, 41]. These approaches belong to the forward-backward class but differ from our proposal in that they consider separable regularization terms, possibly based on distinct learned denoisers acting on different variables. In those works, the notion of block of coordinates is different, as the blocks correspond to distinct variables, e.g., the kernel and the image in blind deconvolution or the dictionary and the sparse coefficients in dictionary learning. In contrast, the PnP setting considered in this paper involves blocks corresponding to different patches of the same image. As a consequence, employing different denoisers for each patch is not feasible, since this would introduce visible artifacts in the reconstruction. Finally, none of the methods in [23, 28, 41] employs line-search strategies for steplength selection; instead, the steplength must be bounded above by a constant related to the Lipschitz constant of the gradient of the fidelity term, which may not be known in practice.

*Contents.* The paper is organized as follows. Section 2 introduces the notations and recalls basic definitions and results on proximal operators. The proposed algorithm is presented in Section 3, together with its application to the PnP framework and an in-depth discussion of related works. The theoretical convergence analysis is provided in Section 4. Numerical experiments are reported in Section 5. Finally, Section 6 is devoted to concluding remarks and future perspectives.

## 2 Preliminaries

The following notations will be used throughout the paper. The symbol  $\|x\| = \sqrt{\langle x, x \rangle}$  stands for the standard Euclidean norm on  $\mathbb{R}^n$ , where  $\langle \cdot, \cdot \rangle$  is the standard Euclidean inner product. The set of real matrices of order  $n$  is denoted by  $\mathbb{R}^{n \times n}$ , and the identity matrix of order  $n$  is indicated by  $I_n$ . The symbol  $\mathcal{S}(n)$  stands for the set of all symmetric matrices of order  $n$ , whereas  $\mathcal{S}_{++}(n)$  denotes the set of real, symmetric and positive definite matrices of order  $n$ . Given  $D \in \mathcal{S}_{++}(n)$ , the norm induced by  $D$  is defined as  $\|x\|_D = \sqrt{\langle x, Dx \rangle}$ . Given  $D_1, D_2 \in \mathcal{S}(n)$ , we say that  $D_1 \preceq D_2$  if and only if  $\langle D_1 x, x \rangle \leq \langle D_2 x, x \rangle$  for all  $x \in \mathbb{R}^n$ .

The following definition is required to efficiently manage blocks of coordinates in the analysis of the proposed framework.

**Definition 2.1.** Let  $U \in \mathbb{R}^{n \times n}$  be a column permutation of the identity matrix and let  $U = [U_1, \dots, U_N]$  be a decomposition of  $U$  in  $N$  submatrices, where each  $U_i \in \mathbb{R}^{n \times n_i}$  is defined with  $n_i = |I_i|$ , being  $I_i \subset \{1, \dots, n\}$  the set of active indexes, and  $\sum_{i=1}^N n_i = n$ .

*Remark.* Any  $x \in \mathbb{R}^n$  can be written as  $x = \sum_{i=1}^N U_i x^{(i)}$ , where  $x^{(i)} = U_i^T x \in \mathbb{R}^{n_i}$  is the  $i$ -th block of coordinates of  $x$ ,  $i = 1, \dots, N$ .

The concept of proximal operator of a function with respect to the norm induced by a real, symmetric, positive definite matrix, is crucial in the proposed framework. Below we report its definition.

**Definition 2.2.** [22, Section 2.3] Let  $\phi : \mathbb{R}^n \rightarrow \mathbb{R} \cup \{\infty\}$  be a proper, lower semicontinuous function,  $\alpha > 0$  and  $D \in \mathcal{S}_{++}(n)$ . The proximal operator of  $\alpha\phi$  with respect to the norm induced by  $D$  is the map  $\text{prox}_{\alpha\phi}^D : \mathbb{R}^n \rightrightarrows \mathbb{R}^n$  defined by

$$\text{prox}_{\alpha\phi}^D(x) = \underset{y \in \mathbb{R}^n}{\text{argmin}} \frac{1}{2} \|y - x\|_D^2 + \alpha\phi(y), \quad \forall x \in \mathbb{R}^n. \quad (8)$$

*Remark.* If  $\phi$  is convex in (8), then  $\text{prox}_{\alpha\phi}^D$  is single-valued, i.e., there exists a unique solution to problem (8); this follows from the fact that the objective function in (8) is strongly convex whenever  $\phi$  is convex. If  $D = I_n$ , then  $\text{prox}_{\alpha\phi}^D = \text{prox}_{\alpha\phi}$ , being  $\text{prox}_{\alpha\phi}$  defined as in (5).

As explained in Section 1, the proposed framework is based on the alternating application of the inertial proximal-gradient step (7) on each block of coordinates. Such a step may be computed

inexactly, for instance when the proximal operator of the function  $\phi$  is not known in closed form. For that reason, we require a well-defined inexactness criterion for the computation of the proximal-gradient point that ensures the convergence of the scheme, while being implementable in a number of practical scenarios. The following definition of proximal inexactness is taken from [13].

**Definition 2.3.** [13, Section 3] Let  $f : \mathbb{R}^n \rightarrow \mathbb{R}$  be continuously differentiable and  $\phi : \mathbb{R}^n \rightarrow \mathbb{R} \cup \{\infty\}$  proper, lower semicontinuous and convex. Choose  $\alpha > 0$ ,  $\beta > 0$ ,  $D \in \mathcal{S}_{++}(n)$  and  $(x, w) \in \mathbb{R}^n \times \mathbb{R}^n$ . Define  $h(\cdot; x, w) : \mathbb{R}^n \rightarrow \mathbb{R} \cup \{\infty\}$  as the strongly convex function given by

$$h(y; x, w) = \langle \nabla f(x) - \frac{\beta}{\alpha} D(x - w), y - x \rangle + \frac{1}{2\alpha} \|y - x\|_D^2 + \phi(y) - \phi(x), \quad \forall y \in \mathbb{R}^n, \quad (9)$$

and the inertial proximal–gradient point as

$$\hat{y} = \operatorname{prox}_{\alpha\phi}^D(x - \alpha D^{-1} \nabla f(x) + \beta(x - w)) = \operatorname{argmin}_{y \in \mathbb{R}^n} h(y; x, w). \quad (10)$$

Given  $\tau \geq 0$ , we call  $\tau$ –approximation of  $\hat{y}$  any point  $\tilde{y} \in \mathbb{R}^n$  satisfying the following condition

$$h(\tilde{y}; x, w) \leq \left( \frac{2}{2 + \tau} \right) h(\hat{y}; x, w). \quad (11)$$

Such a point is denoted with  $\tilde{y} \approx_\tau \hat{y}$ .

*Remark.* Function  $h(\cdot; x, w)$  in (9) is defined so that  $h(\hat{y}; x, w) \leq h(x; x, w) = 0$ . From this remark, it also follows that the inexactness condition (11) is well-defined and  $h(\tilde{y}; x, w) \leq 0$ . If  $\tau = 0$ , then  $\tilde{y} = \hat{y}$ , i.e., the  $\tau$ –approximation coincides with the unique proximal–gradient point; otherwise, if  $\tau > 0$ , we have an approximation  $\tilde{y}$  that gets closer to  $\hat{y}$  as  $\tau$  tends to zero (coarser as  $\tau$  tends to infinity, respectively).

The following result estimates the mutual distance between the points  $x, \hat{y}, \tilde{y}$  in terms of the function value  $-h(\tilde{y}; x, w)$ . It is taken from [13] and follows by slightly modifying the arguments in [11, Lemma 8], whose proof was given under the assumption  $D = I_n$ .

**Lemma 2.1.** [13, Lemma 9] Let  $f : \mathbb{R}^n \rightarrow \mathbb{R}$  be continuously differentiable and  $\phi : \mathbb{R}^n \rightarrow \mathbb{R} \cup \{\infty\}$  proper, lower semicontinuous and convex. Choose  $0 < \alpha \leq \alpha_{\max}$ ,  $\beta > 0$ ,  $\mu > 0$ ,  $D \in \mathcal{S}_{++}(n)$  with  $\frac{1}{\mu} I_n \preceq D \preceq \mu I_n$  and  $(x, w) \in \mathbb{R}^n \times \mathbb{R}^n$ . Let  $h(\cdot; x, w)$  be the function in (9) and  $\hat{y}, \tilde{y}$  the points defined as in (10)–(11). Then, the following inequalities hold:

$$\|\hat{y} - x\|^2 \leq 2\alpha_{\max}\mu \left(1 + \frac{\tau}{2}\right) (-h(\tilde{y}; x, w)) \quad (12)$$

$$\|\tilde{y} - \hat{y}\|^2 \leq \alpha_{\max}\mu\tau (-h(\tilde{y}; x, w)) \quad (13)$$

$$\|\tilde{y} - x\|^2 \leq 2\alpha_{\max}\mu \left( \sqrt{1 + \frac{\tau}{2}} + \sqrt{\frac{\tau}{2}} \right)^2 (-h(\tilde{y}; x, w)). \quad (14)$$

We now recall the definition of the Kurdyka–Łojasiewicz (KL) inequality [9]. Such a definition is usually given for proper, lower semicontinuous functions; however, here we consider the definition only for differentiable functions, as it is our case of interest.

**Definition 2.4.** [9, Definition 3] Let  $F : \mathbb{R}^n \rightarrow \mathbb{R}$  be a continuously differentiable function. The function  $F$  satisfies the Kurdyka–Łojasiewicz (KL) inequality at the point  $x^* \in \mathbb{R}^n$  if there exist  $\nu > 0$ , a neighborhood  $U$  of  $x^*$ , and a continuous concave function  $\xi : [0, \nu) \rightarrow [0, +\infty)$  such that  $\xi(0) = 0$ ,  $\xi \in C^1((0, \nu))$ ,  $\xi'(s) > 0$  for all  $s \in (0, \nu)$ , and the following inequality holds

$$\xi'(F(x) - F(x^*)) \|\nabla F(x)\| \geq 1, \quad (15)$$

for all  $x \in U \cap \{y \in \mathbb{R}^n : F(x^*) < F(y) < F(x^*) + \nu\}$ . If  $F$  satisfies the KL inequality for all  $x^* \in \mathbb{R}^n$ , then  $F$  is called a KL function.

The KL inequality (15) holds for several objective functions appearing in classical signal and image processing models, see e.g. [9, 46]. Notably, such an inequality holds also for most finite dimensional deep learning models, including those involving functions of the form (3) [16].

### 3 A block-coordinate inexact line-search framework for non-separable optimization

In this section, we introduce Block-PHILA - Block Proximal Heavy-ball Inexact Line-search Algorithm - the novel block-coordinate framework that lies at the core of our proposed PnP approach. First, we describe Block-PHILA (Section 3.1); then we compare it with other block-coordinate approaches already existing in the literature (Section 3.2); finally, we detail its application to the PnP framework (Section 3.3).

#### 3.1 The proposed framework

Block-PHILA is a block-coordinate framework suitable for problems of the form (1) under the blanket assumptions stated in Assumption 1.

**Assumption 1.** *The functions  $f$  and  $\phi$  appearing in (1) satisfy the following conditions.*

(i) *The function  $f : \mathbb{R}^n \rightarrow \mathbb{R}$  is continuously differentiable.*

(ii) *Given any matrix  $U = [U_1, \dots, U_N]$  defined as in Definition 2.1, the function  $\phi : \mathbb{R}^n \rightarrow \mathbb{R} \cup \{\infty\}$  is convex along coordinates, i.e., the function*

$$\phi_i^x : \mathbb{R}^{n_i} \rightarrow \mathbb{R} \cup \{\infty\}, \quad \phi_i^x(z) = \phi(x + U_i(z - U_i^T x)), \quad \forall z \in \mathbb{R}^{n_i}, \quad (16)$$

*is convex for all  $x \in \mathbb{R}^n$  and  $i = 1, \dots, N$ .*

(iii) *The function  $F = f + \phi$  is bounded from below, i.e., there exists  $F_{low} \in \mathbb{R}$  such that  $F \geq F_{low}$ .*

We start by summarizing the steps of the proposed framework. At each iteration  $k \in \mathbb{N}$ , Block-PHILA cyclically selects the index  $i_k \in \{1, \dots, N\}$ , two parameters  $\alpha_k > 0$ ,  $\beta_k > 0$ , and a symmetric positive definite matrix  $D_k \in \mathbb{R}^{n_{i_k} \times n_{i_k}}$ . Starting from the current iterate  $x_k$ , the algorithm performs a gradient step on  $f$  restricted to the  $i_k$ -th block of coordinates, possibly equipped with an inertial term combining the two previous updates on that block. Then, a proximal step is performed on the function  $\phi$  restricted to the subspace generated by the columns of  $U_{i_k}$ . Note that  $\alpha_k$  and  $D_k$  define the variable metric of the proximal-gradient operator, whereas  $\beta_k$  scales the inertial term. Furthermore, such a block proximal-gradient point can be approximately computed according to a well-posed inexactness condition, which is implementable in some cases of interest. Once the proximal-gradient point is computed, the new iterate  $x_{k+1} \in \mathbb{R}^n$  is detected by means of a line-search procedure that enforces the sufficient decrease of a suitable merit function along the search direction.

We now report Block-PHILA in full detail in Algorithm 1.

Let us describe Block-PHILA step-by-step. Prior to the beginning of the iterative procedure, the framework requires the user to select the following parameters:

- $x_0 \in \mathbb{R}^n$  and  $x_{-1} = \dots = x_{-N} = x_0$  as the  $N + 1$  initial guesses;
- $0 < \alpha_{\min} \leq \alpha_{\max}$  as the lower and upper bounds, respectively, for the steplengths  $\{\alpha_k\}_{k \in \mathbb{N}}$ ;
- $\beta_{\max} > 0$  defining the interval  $[0, \beta_{\max}]$  constraining the inertial parameters  $\{\beta_k\}_{k \in \mathbb{N}}$ ;
- $\mu > 0$  defining the space to which the scaling matrices  $\{D_k\}_{k \in \mathbb{N}}$  belong to, i.e., the space of all symmetric, positive definite matrices whose eigenvalues are in the interval  $[\frac{1}{\mu}, \mu]$ ;
- $\tau \geq 0$  controlling the level of accuracy in the computation of the inexact proximal point;
- $\gamma > 0$ ,  $\delta \in (0, 1)$ ,  $\sigma \in (0, 1)$  as the line-search parameters.

---

**Algorithm 1** Block Proximal Heavy-ball Inexact Line-search Algorithm (Block-PHILA)

Choose  $x_0 \in \mathbb{R}^n$ ,  $x_{-1} = \dots = x_{-N} = x_0$ ,  $0 < \alpha_{\min} \leq \alpha_{\max}$ ,  $\beta_{\max} > 0$ ,  $\mu > 0$ ,  $\tau \geq 0$ ,  $\gamma > 0$ ,  $\delta, \sigma \in (0, 1)$ .  
 FOR  $k = 0, 1, \dots$

STEP 1. Set  $i_k = \text{mod}(k, N) + 1$ .

STEP 2. Choose  $\alpha_k \in [\alpha_{\min}, \alpha_{\max}]$ ,  $\beta_k \in [0, \beta_{\max}]$ ,  $D_k \in \mathcal{S}_{++}(n_{i_k})$  such that  $\frac{1}{\mu} I_{n_{i_k}} \preceq D_k \preceq \mu I_{n_{i_k}}$ .

STEP 3. Let  $\phi_{i_k}^{x_k}(z) = \phi(x_k + U_{i_k}(z - U_{i_k}^T x_k))$  and compute

$$\tilde{y}_k \approx_{\tau} \text{prox}_{\alpha_k \phi_{i_k}^{x_k}}^{D_k} (U_{i_k}^T (x_k + \beta_k (x_k - x_{k-N})) - \alpha_k D_k^{-1} U_{i_k}^T \nabla f(x_k)). \quad (17)$$

STEP 4. Set  $d_k = \tilde{y}_k - U_{i_k}^T x_k$  and compute

$$\begin{aligned} h_k(\tilde{y}_k) &= \langle U_{i_k}^T \nabla f(x_k) - \frac{\beta_k}{\alpha_k} D_k U_{i_k}^T (x_k - x_{k-N}), d_k \rangle \\ &+ \frac{1}{2\alpha_k} \|d_k\|_{D_k}^2 + \phi_{i_k}^{x_k}(\tilde{y}_k) - \phi_{i_k}^{x_k}(U_{i_k}^T x_k). \end{aligned} \quad (18)$$

STEP 5. Compute the smallest non-negative integer  $m_k$  such that

$$F(x_k + \delta^{m_k} U_{i_k} d_k) + \frac{\gamma}{2} \|\delta^{m_k} d_k\|^2 \leq F(x_k) + \frac{\gamma}{2} \|U_{i_k}^T (x_k - x_{k-N})\|^2 + \sigma \delta^{m_k} h_k(\tilde{y}_k), \quad (19)$$

and set  $\lambda_k = \delta^{m_k}$ .

STEP 6. Compute

$$x_{k+1} = x_k + \begin{cases} U_{i_k} d_k, & \text{if } F(x_k + U_{i_k} d_k) + \frac{\gamma}{2} \|d_k\|^2 < F(x_k + \lambda_k U_{i_k} d_k) + \frac{\gamma}{2} \lambda_k^2 \|d_k\|^2 \\ \lambda_k U_{i_k} d_k, & \text{otherwise.} \end{cases} \quad (20)$$


---

At STEPS 1-2, we cyclically select the block index  $i_k = \text{mod}(k, N) + 1$ , and compute the steplength  $\alpha_k \in [\alpha_{\min}, \alpha_{\max}]$ , the inertial parameter  $\beta_k \in [0, \beta_{\max}]$  and the scaling matrix  $D_k \in \mathcal{S}_{++}(n_{i_k})$  with  $\frac{1}{\mu} I_{n_{i_k}} \preceq D_k \preceq \mu I_{n_{i_k}}$ . These three parameters can be computed according to any chosen updating rule and are intended to make the  $k$ -th block step faster than standard implementations employing either fixed parameters or local estimates of the Lipschitz constant.

STEP 3 aims at computing an inexact proximal–gradient step with respect to the  $i_k$ -th block of coordinates  $x^{(i_k)} = U_{i_k}^T x$ , while fixing the other blocks as the ones of the current iterate  $x_k$ . In detail, we denote with  $\phi_{i_k}^{x_k} : \mathbb{R}^{n_{i_k}} \rightarrow \mathbb{R} \cup \{\infty\}$  the restriction of the function  $\phi$  to the subspace generated by the columns of  $U_{i_k}$ , i.e.,

$$\phi_{i_k}^{x_k}(y) = \phi(x_k + U_{i_k}(y - U_{i_k}^T x_k)), \quad \forall y \in \mathbb{R}^{n_{i_k}}. \quad (21)$$

We consider the block proximal–gradient point  $\hat{y}_k \in \mathbb{R}^{n_{i_k}}$  with parameters  $\alpha_k, \beta_k, D_k$  defined as

$$\hat{y}_k = \text{prox}_{\alpha_k \phi_{i_k}^{x_k}}^{D_k} (U_{i_k}^T (x_k + \beta_k (x_k - x_{k-N})) - \alpha_k D_k^{-1} U_{i_k}^T \nabla f(x_k)). \quad (22)$$

Note that the matrix  $D_k^{-1}$  has the role of scaling the term  $-U_{i_k}^T \nabla f(x_k)$ , namely the  $i_k$ -th block of coordinates of the negative gradient at  $x_k$ , whereas  $\beta_k$  scales the inertial term  $U_{i_k}^T (x_k - x_{k-N})$ . By Definition 2.2 of proximal operator, the point  $\hat{y}_k$  can be characterized as follows

$$\begin{aligned} \hat{y}_k &= \underset{y \in \mathbb{R}^{n_{i_k}}}{\text{argmin}} \frac{1}{2} \|y - U_{i_k}^T (x_k + \beta_k (x_k - x_{k-N})) + \alpha_k D_k^{-1} U_{i_k}^T \nabla f(x_k)\|_{D_k}^2 + \alpha_k \phi_{i_k}^{x_k}(y) \\ &= \underset{y \in \mathbb{R}^{n_{i_k}}}{\text{argmin}} \langle U_{i_k}^T \nabla f(x_k) - \frac{\beta_k}{\alpha_k} D_k U_{i_k}^T (x_k - x_{k-N}), y - U_{i_k}^T x_k \rangle + \frac{1}{2\alpha_k} \|y - U_{i_k}^T x_k\|_{D_k}^2 + \phi_{i_k}^{x_k}(y) \\ &= \underset{y \in \mathbb{R}^{n_{i_k}}}{\text{argmin}} h_k(y), \end{aligned} \quad (23)$$

where  $h_k : \mathbb{R}^{n_{i_k}} \rightarrow \mathbb{R} \cup \{\infty\}$  is the function defined as

$$\begin{aligned} h_k(y) &= \langle U_{i_k}^T \nabla f(x_k) - \frac{\beta_k}{\alpha_k} D_k U_{i_k}^T (x_k - x_{k-N}), y - U_{i_k}^T x_k \rangle \\ &\quad + \frac{1}{2\alpha_k} \|y - U_{i_k}^T x_k\|_{D_k}^2 + \phi_{i_k}^{x_k}(y) - \phi_{i_k}^{x_k}(U_{i_k}^T x_k), \quad \forall y \in \mathbb{R}^{n_{i_k}}. \end{aligned} \quad (24)$$

Note that  $h_k$  is defined by shifting the function appearing in (23) by the constant  $-\phi_{i_k}^{x_k}(U_{i_k}^T x_k)$ , so that  $h_k(U_{i_k}^T x_k) = 0$  and  $h_k(\hat{y}_k) \leq h_k(U_{i_k}^T x_k) = 0$ . Then, given  $\tau > 0$ , Block-PHILA computes an inexact inertial proximal–gradient point  $\tilde{y}_k \in \mathbb{R}^{n_{i_k}}$  complying with the following inexactness condition

$$h_k(\tilde{y}_k) \leq \left( \frac{2}{2 + \tau} \right) h_k(\hat{y}_k). \quad (25)$$

Note that the search of a point  $\tilde{y}_k$  complying with (25) is feasible since  $h_k(\hat{y}_k) \leq 0$ . If  $\tau = 0$ , then  $\tilde{y}_k = \hat{y}_k$ , meaning that Block-PHILA computes the proximal–gradient point in an exact manner; viceversa, if  $\tau > 0$ , then Block-PHILA computes an inexact point which gets closer and closer to  $\tilde{y}_k$  as  $\tau$  tends to zero.

In STEP 4, Block-PHILA defines the search direction  $d_k = \tilde{y}_k - U_{i_k}^T x_k$  and keeps track of the value  $h_k(\tilde{y}_k)$ . Then, STEP 5 performs a line-search along the direction  $U_{i_k} d_k$  in order to satisfy an appropriate Armijo-like condition. More precisely, Block-PHILA computes the parameter  $\lambda_k = \delta^{m_k} \in (0, 1]$ , where  $m_k$  is the smallest non-negative integer such that

$$F(x_k + \delta^{m_k} U_{i_k} d_k) + \frac{\gamma}{2} \|\delta^{m_k} d_k\|^2 \leq F(x_k) + \frac{\gamma}{2} \|U_{i_k}^T (x_k - x_{k-N})\|^2 + \sigma \delta^{m_k} h_k(\tilde{y}_k).$$

In general, the above condition does not imply the decrease of the objective function  $F$  from one iteration to the other; nonetheless, since  $h_k(\tilde{y}_k) \leq 0$ , the above condition forces the quantity  $F(x_k +$

$\lambda_k U_{i_k} d_k) + \frac{\gamma}{2} \lambda_k^2 \|d_k\|^2$  to be smaller than  $F(x_k) + \frac{\gamma}{2} \|U_{i_k}^T(x_k - x_{k-N})\|^2$ . We will see in Section 4 (precisely in Lemma 4.3) that STEP 5 is actually equivalent to imposing the sufficient decrease of a suitable merit function  $\Psi$  along the sequence  $\{(x_k, x_{k-1}, \dots, x_{k-N})\}_{k \in \mathbb{N}}$  of  $N + 1$  successive iterates.

Finally, in STEP 6, the new iterate  $x_{k+1}$  is set as either the convex combination  $x_k + \lambda_k U_{i_k} d_k$  or the point  $x_k + U_{i_k} d_k$ , depending on whether the quantity  $F(x_k + \lambda_k U_{i_k} d_k) + \frac{\gamma}{2} \lambda_k^2 \|d_k\|^2$  appearing in the Armijo-like condition is smaller than the quantity  $F(x_k + U_{i_k} d_k) + \frac{\gamma}{2} \|d_k\|^2$  computed for the first trial point of the backtracking procedure.

### 3.2 Related works

The Block-PHILA method can be viewed as an alternating block-coordinate version of the Proximal Heavy-ball Inexact Line-search Algorithm (PHILA) proposed in [13]. Specifically, at each iteration, Block-PHILA applies a PHILA step to one block of coordinates  $x^{(i)}$  at a time while keeping all other blocks fixed. Extending PHILA to the block-coordinate setting is non-trivial, as it requires a careful design of the inertial term across the blocks and the suitable definition of a merit function that decreases throughout the iterations. Regarding the latter, the decreasing merit function used to prove convergence in PHILA coincides with the one employed in the algorithm's line-search. In contrast, the definition of the merit function in Block-PHILA, while still relying on the line-search inequality, must be adapted in order to take into account the block-coordinate structure of the algorithm (see Lemma 4.3).

Beyond Block-PHILA, several other block-coordinate proximal-gradient methods have been proposed for minimizing a possibly non-convex objective function of the form (1), accelerated either by inertial terms or by variable metrics [12, 19, 22, 25, 34, 36, 37, 46, 47]. However, these methods (i) do not combine inertial and variable metric acceleration strategies simultaneously, and (ii) are tailored for problems of the form (1) where the function  $\phi$  consists of a sum of separable and possibly non-differentiable components. In contrast, Block-PHILA allows the combination of inertial and variable metric strategies, and is designed to handle objective functions of the form (1) where  $\phi$  is differentiable and possibly non-separable. Such an assumption on  $\phi$  is crucial in practical applications such as the Plug-and-Play framework, where the optimization problem typically involves the sum of two differentiable but non-separable terms. Further details on how Block-PHILA can be employed in Plug-and-Play scenarios are provided in Section 3.3.

On the other hand, there are few block-coordinate descent methods for composite objective functions as in (1) where the second term can be supposed non-separable [1, 18, 24, 26, 30]. In [1], the authors study the minimization of the sum of a quadratic function and a non-smooth, non-separable function and propose a coordinate gradient descent-type method based on the forward-backward envelope to smooth the original problem. Chorobura and Necoara [18] propose a coordinate proximal-gradient algorithm where, for problem (1), the algorithm updates the variables by performing a descent step using selected components of the gradient of  $f$ , followed by a proximal step applied to a function restricted to the corresponding subspace, similarly to the one in (21). Furthermore, given the problem (1), [24, 26] study proximal coordinate descent whose general iteration reads as

$$x_{k+1} \in \text{prox}_{\alpha\phi}(\mathcal{C}(x_k - \alpha\nabla f(x_k))), \quad (26)$$

where  $\mathcal{C}(\cdot)$  is a map defined by the randomly chosen subspace at the current iteration. The algorithm proposed in [30], tailored for problem (1) with general non-convex  $\phi$ , is similar to that in (26), but  $\mathcal{C}(\cdot)$  is simply the identity map; here only a proper subset of indices  $I_{k+1} \subseteq \{1, \dots, N\}$  is selected and the corresponding block of coordinates is updated by means of (26), leaving the remaining coordinates unchanged by setting  $x_{k+1}^{(i)} = x_k^{(i)}$ ,  $i \in \{1, \dots, N\} \setminus I_{k+1}$ . It is also worth noting that [24, 26] use only a sketch of the gradient of  $f$  restricted to the selected subspace, while [30] assumes that  $f$  itself is separable.

We remark that none of the early mentioned approaches for non-separable optimization adopts a line-search strategy to select the step length, often leading to restrictive bounds on this parameter.

They also do not consider inertial and/or variable metric acceleration strategies, and they do not allow for an inexact computation of the proximal point. Moreover in [1, 24, 26, 30], the proximal update is not computed coordinate-wise, but instead requires computing a block of coordinates of the full proximal point, by implicitly assuming that the function  $\phi$  in (1) admits a low-complexity proximal mapping.

To the best of our knowledge, Block-PHILA is the first block-coordinate proximal–gradient method designed for non-convex and non-separable problems that offers provable convergence guarantees, includes a line-search strategy to adaptively select the steplength without impractical constraints, and can potentially be accelerated by jointly using inertial steps and a variable metric underlying the iterations.

### 3.3 Application to the Plug-and-Play framework

This section is devoted to detail how Algorithm 1 can be applied to image restoration problems of the form

$$\operatorname{argmin}_{x \in \mathbb{R}^n} \phi(x) + f(x) \equiv \phi(x) + \lambda g_\sigma(x), \quad (27)$$

where  $\phi : \mathbb{R}^n \rightarrow \mathbb{R}$  is a data fidelity term,  $g_\sigma : \mathbb{R}^n \rightarrow \mathbb{R}$  is defined in (3), and  $\lambda > 0$  is a regularization parameter.

First, we specify that we consider a collection of decomposition submatrices  $\{U_i\}_{i=1}^N$  that partition the image into blocks of contiguous pixels. For example, an image can be decomposed into four non-overlapping quadrants, each representing one block of coordinates. In the following, we show how the computation of  $\nabla f(x_k)$  restricted to each block in (17) can be efficiently handled.

#### 3.3.1 Block GS denoiser

In this section, we describe how it is possible to reduce the memory overhead required to perform the computation of  $U_{i_k}^T \nabla g_\sigma(x_k)$  through the derivation of a restricted block version of the GS denoiser. More in detail, in view of (6),  $\nabla g_\sigma$  depends on  $J_{N_\sigma}(x)$ , whose computation requires storing the entire computational graph in order to perform the backward pass. The memory needed to perform this intermediate step depends on the size of the images, thus limiting the usability of GS denoisers in limited resources scenarios, for example on a laptop or on a smartphone. For this reason, we introduce a variant of the GS denoisers, named block GS denoisers (BGS), in order to perform the denoising step on a single block of the image with a reduced memory footprint on the GPU, avoiding to compute the entire  $J_{N_\sigma}(x)$  and the subsequent extraction of the rows associated to the selected block. This construction is crucial for the implementation of Block-PHILA in the considered PnP framework.

We recall the concept of receptive field for a convolutional neural network in order to derive our BGS denoisers. In general, the receptive field refers to the region of the input that influences the single pixel in the output. More specifically, the receptive field of a simple convolutional layer is equal to its kernel size [31]. The theoretical receptive field of a convolutional neural network (CNN) can be computed by considering how the size, stride, and padding of the kernel of each layer combine to determine the size of the input region that affects a specific output location. Mathematically, this means that a single pixel in the output does not depend on the pixels outside of its receptive field. This independence is reflected also in the partial derivatives of the neural network.

In our setting, we consider the function  $N_\sigma$  defined as a convolutional neural network, specifically employing a UNet architecture as in [29]. In general, CNN architectures enable the network to handle images of varying sizes without requiring modification to the model parameters or structure. Let us consider  $i_k \in \{1, \dots, N\}$  as a block selection index and  $\hat{i} \in \{1, \dots, N\}$ . Computationally, if we are interested in the partial derivatives of  $N_\sigma$  in the  $\hat{i}$ -th component there are two cases

- $\frac{\partial N_\sigma(x)_r}{\partial x_j} = 0$ , if the  $j$ -th pixel of  $x$  is not in the receptive field associated to the pixel  $r$  in the block  $\hat{i}$ ;

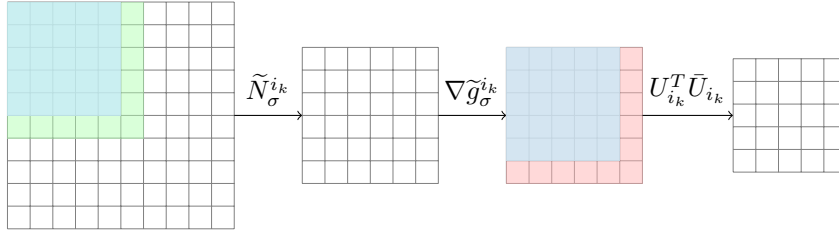


Figure 1: Example of block GS denoiser action.

- $\frac{\partial N_\sigma(x)_r}{\partial x_j} \neq 0$ , otherwise.

For each block index  $i_k$  we can define the restricted neural network acting on a smaller patch of the image, namely  $\tilde{N}_\sigma^{i_k} : \mathbb{R}^{n_i+o_k} \rightarrow \mathbb{R}^{n_i+o_k}$ , where  $o_k$  denotes the number of additional pixels considered in the padded block of coordinates, such that the following condition holds

$$U_{i_k}^T N_\sigma(x) = U_{i_k}^T \bar{U}_{i_k} \tilde{N}_\sigma^{i_k} (\bar{U}_{i_k}^T x), \quad (28)$$

where  $\bar{U}_{i_k}$  denotes the masking matrix which considers the indexes of the pixels within the receptive field associated to the pixels in  $I_{i_k}$ . In practice, this means that extracting a block of coordinates of the neural network output  $N_\sigma(x)$  is equivalent to extracting the same block of the restricted neural network output  $\tilde{N}_\sigma^{i_k} (\bar{U}_{i_k}^T x)$ . Now, considering the following potential function:

$$\tilde{g}_\sigma^{i_k}(x) = \frac{1}{2} \|\bar{U}_{i_k}^T x - \tilde{N}_\sigma^{i_k} (\bar{U}_{i_k}^T x)\|^2 \quad (29)$$

we can compute its gradient

$$\nabla \tilde{g}_\sigma^{i_k}(x) = \bar{U}_{i_k} \left( \bar{U}_{i_k}^T x - \tilde{N}_\sigma^{i_k} (\bar{U}_{i_k}^T x) - J_{\tilde{N}_\sigma^{i_k}} (\bar{U}_{i_k}^T x)^T (\bar{U}_{i_k}^T x - \tilde{N}_\sigma^{i_k} (\bar{U}_{i_k}^T x)) \right). \quad (30)$$

We point out that the computation of  $\tilde{N}_\sigma^{i_k}$  and its associated Jacobian  $J_{\tilde{N}_\sigma^{i_k}}$  require less memory since its input belongs to a smaller space. Furthermore, the  $i_k$ -th block of coordinates of  $\nabla \tilde{g}_\sigma^{i_k}(x)$  writes as

$$\begin{aligned} U_{i_k}^T \nabla \tilde{g}_\sigma^{i_k}(x) &= U_{i_k}^T \bar{U}_{i_k} \left( \bar{U}_{i_k}^T x - \tilde{N}_\sigma^{i_k} (\bar{U}_{i_k}^T x) - J_{\tilde{N}_\sigma^{i_k}} (\bar{U}_{i_k}^T x)^T (\bar{U}_{i_k}^T x - \tilde{N}_\sigma^{i_k} (\bar{U}_{i_k}^T x)) \right) \\ &= U_{i_k}^T \left( x - N_\sigma(x) - \bar{U}_{i_k} J_{\tilde{N}_\sigma^{i_k}} (\bar{U}_{i_k}^T x)^T (\bar{U}_{i_k}^T x - \tilde{N}_\sigma^{i_k} (\bar{U}_{i_k}^T x)) \right), \end{aligned} \quad (31)$$

where we used (28) and property  $U_{i_k}^T \bar{U}_{i_k} \bar{U}_{i_k}^T = U_{i_k}^T$  of the masking matrices. Finally, noting that

$$U_{i_k}^T \bar{U}_{i_k} J_{\tilde{N}_\sigma^{i_k}} (\bar{U}_{i_k}^T x)^T (\bar{U}_{i_k}^T x - \tilde{N}_\sigma^{i_k} (\bar{U}_{i_k}^T x)) = U_{i_k}^T J_{N_\sigma}(x)^T (x - N_\sigma(x)), \quad (32)$$

and plugging (32) into (31), we conclude that

$$U_{i_k}^T \nabla \tilde{g}_\sigma^{i_k}(x) = U_{i_k}^T \nabla g_\sigma(x). \quad (33)$$

In Figure 1, we present a diagram illustrating the dimensions of the tensors involved in the gradient computation under the proposed approach, considering a set of masking matrices that select one image quadrant at a time.

## 4 Convergence analysis of Block-PHILA

In this section, we carry out the convergence analysis of Algorithm 1. In the first part, we show a sub-linear convergence rate and the stationarity of limit points under Assumption 1 and some smoothness requirements on both  $f$  and  $\phi$  (Section 4.1). Then, we prove the convergence of the whole sequence to a stationary point and related convergence rates, by additionally assuming that some appropriate surrogate functions of  $F$  satisfy the KL property on their domains (Section 4.2).

## 4.1 Stationarity of limit points and sublinear rate

We start by deriving the following lemma, which will be frequently used in the convergence analysis of Algorithm 1.

**Lemma 4.1.** *Suppose Assumption 1 holds. For all  $k \in \mathbb{N}$ , the following inequalities hold:*

$$\|\hat{y}_k - U_{i_k}^T x_k\|^2 \leq 2\alpha_{\max}\mu \left(1 + \frac{\tau}{2}\right) (-h_k(\tilde{y}_k)) \quad (34)$$

$$\|\tilde{y}_k - \hat{y}_k\|^2 \leq \alpha_{\max}\mu\tau(-h_k(\tilde{y}_k)) \quad (35)$$

$$\|d_k\|^2 = \|\tilde{y}_k - U_{i_k}^T x_k\|^2 \leq 2\alpha_{\max}\mu \left(\sqrt{1 + \frac{\tau}{2}} + \sqrt{\frac{\tau}{2}}\right)^2 (-h_k(\tilde{y}_k)). \quad (36)$$

*Proof.* In Lemma 2.1, set  $f(y) = f(x_k + U_{i_k}(y - x_k))$ ,  $\phi(y) = \phi_{i_k}^{x_k}(y)$ ,  $x = U_{i_k}^T x_k$ ,  $w = U_{i_k}^T x_{k-N}$ ,  $\alpha = \alpha_k$ ,  $\beta = \beta_k$  and  $D = D_k$ . By using these settings, we have  $\hat{y} = \hat{y}_k$ ,  $\tilde{y} = \tilde{y}_k$ , with  $\hat{y}_k, \tilde{y}_k$  defined in (22)-(25) and  $h(\cdot; x, w) = h_k(\cdot)$ , being  $h_k$  defined in (24). Hence, the inequalities (34)-(35)-(36) follow as mere applications of inequalities (12)-(13)-(14) from Lemma 2.1.  $\square$

Next, we state the well-posedness of the line-search performed at STEP 5 of Algorithm 1. To this aim, we require the function  $f$  to have a Lipschitz continuous gradient. Note that such an assumption holds for the function  $f = \lambda g_\sigma$ , being  $\lambda > 0$  and  $g_\sigma$  defined in (3) and appearing in the PnP model (27), provided that the neural network  $N_\sigma$  in (3) is given by the composition of continuously differentiable functions whose derivatives are bounded and Lipschitz [29, Proposition 2], as is the case of the convolutional neural network adopted in the numerical experiments of Section 5.

**Assumption 2.**  $\nabla f$  is Lipschitz continuous with constant  $L_f > 0$ , i.e.,

$$\|\nabla f(x) - \nabla f(y)\| \leq L_f \|x - y\|, \quad \forall x, y \in \mathbb{R}^n. \quad (37)$$

**Lemma 4.2.** *Suppose Assumptions 1-2 hold.*

(i) *For all  $k \in \mathbb{N}$ , the line-search defined at STEP 5 of Algorithm 1 terminates in a finite number of steps, i.e.,  $m_k < \infty$  for all  $k \in \mathbb{N}$ .*

(ii) *There exists  $\lambda_{\min} > 0$  such that*

$$\lambda_k = \delta^{m_k} \geq \lambda_{\min}, \quad \forall k \in \mathbb{N}.$$

*Proof.* The line-search at STEP 5 of Algorithm 1 is exactly the one described in [13, Algorithm 1] when applied to the functions  $f_0(\cdot) = f(x_k + U_{i_k}(\cdot - U_{i_k}^T x_k))$  and  $f_1(\cdot) = \phi_{i_k}^{x_k}(\cdot)$ , using the iterates  $x^{(k)} = U_{i_k}^T x_k$  and  $x^{(k-1)} = U_{i_k}^T x_{k-N}$ , and the search direction  $d^{(k)} = \tilde{y}_k - U_{i_k}^T x_k$ . Hence, the thesis follows by applying [13, Lemma 12].  $\square$

We now show that the line-search at STEP 5 enforces the sufficient decrease of a suitable merit function  $\Psi$ , which incorporates both the objective function  $F$  and the information related to the inertial steps. Similar merit functions have previously appeared in the analysis of other block-coordinate proximal-gradient methods with inertial terms [34, 36].

**Lemma 4.3.** *Suppose Assumptions 1-2 hold. Define the merit function*

$$\Psi(z_1, \dots, z_{N+1}) = F(z_1) + \frac{\gamma}{2} \sum_{i=1}^N \|z_i - z_{i+1}\|^2, \quad z_i \in \mathbb{R}^n, \quad i = 1, \dots, n+1. \quad (38)$$

*Then, the following statements hold.*

(i) For all  $k \in \mathbb{N}$ , we have

$$\Psi(x_{k+1}, x_k, \dots, x_{k-N+1}) \leq \Psi(x_k, x_{k-1}, \dots, x_{k-N}) + \sigma \lambda_{\min} h_k(\tilde{y}_k). \quad (39)$$

(ii) We have

$$\sum_{k=0}^{\infty} (-h_k(\tilde{y}_k)) < \infty. \quad (40)$$

*Proof.* (i) We start by observing that

$$U_{i_k}^T(x_k - x_{k-N}) = U_{i_k}^T(x_{k-N+1} - x_{k-N}), \quad (41)$$

as the  $i_k$ -th block of coordinates is never updated in none of the previous  $N-1$  iterations  $k-1, k-2, \dots, k-N+1$  preceding the  $k$ -th iteration. Furthermore  $\|U_{i_k}^T(x_{k-N+1} - x_{k-N})\| = \|x_{k-N+1} - x_{k-N}\|$  as the  $i_k$ -th block of coordinates is the only one to be updated at iteration  $k-N$ . Then, the Armijo-like condition (19) in STEP 5 of Algorithm 1 rewrites as

$$F(x_k + \lambda_k U_{i_k} d_k) + \frac{\gamma}{2} \lambda_k^2 \|d_k\|^2 \leq F(x_k) + \frac{\gamma}{2} \|x_{k-N+1} - x_{k-N}\|^2 + \sigma \lambda_k h_k(\tilde{y}_k).$$

By summing the quantity  $\frac{\gamma}{2} \sum_{i=1}^{N-1} \|x_{k-i+1} - x_{k-i}\|^2$  to both sides of the previous inequality, we obtain

$$F(x_k + \lambda_k U_{i_k} d_k) + \frac{\gamma}{2} \lambda_k^2 \|d_k\|^2 + \frac{\gamma}{2} \sum_{i=1}^{N-1} \|x_{k-i+1} - x_{k-i}\|^2 \leq F(x_k) + \frac{\gamma}{2} \sum_{i=1}^N \|x_{k-i+1} - x_{k-i}\|^2 + \sigma \lambda_k h_k(\tilde{y}_k).$$

By recalling the definition of the merit function (38), the Armijo-like condition is easily rewritten as

$$\Psi(x_k + \lambda_k U_{i_k} d_k, x_k, x_{k-1}, \dots, x_{k-N+1}) \leq \Psi(x_k, x_{k-1}, x_{k-2}, \dots, x_{k-N}) + \sigma \lambda_k h_k(\tilde{y}_k). \quad (42)$$

Furthermore, by following a similar reasoning as the one just conducted for the Armijo-like condition, one can rewrite STEP 6 in terms of the function  $\Psi$  as

$$x_{k+1} = x_k + \begin{cases} U_{i_k} d_k, & \text{if } \Psi(x_k + U_{i_k} d_k, x_k, \dots, x_{k-N+1}) < \Psi(x_k + \lambda_k U_{i_k} d_k, x_k, \dots, x_{k-N+1}) \\ \lambda_k U_{i_k} d_k, & \text{otherwise.} \end{cases} \quad (43)$$

Hence, in both cases, the following property holds

$$\Psi(x_{k+1}, x_k, x_{k-1}, \dots, x_{k-N+1}) \leq \Psi(x_k + \lambda_k U_{i_k} d_k, x_k, x_{k-1}, \dots, x_{k-N+1}). \quad (44)$$

Combining (44) and (42) leads to the inequality

$$\Psi(x_{k+1}, x_k, \dots, x_{k-N+1}) \leq \Psi(x_k, x_{k-1}, \dots, x_{k-N}) + \sigma \lambda_k h_k(\tilde{y}_k). \quad (45)$$

By recalling that  $h_k(\tilde{y}_k) \leq 0$  and applying Lemma 4.2(ii) to (45), we obtain the thesis of item (i).

(ii) By summing inequality (39) for  $k = 0, \dots, K$ , and noting the telescopic sum at the right-hand side, we get the following

$$\begin{aligned} \sigma \lambda_{\min} \sum_{k=0}^K (-h_k(\tilde{y}_k)) &\leq \sum_{k=0}^K (\Psi(x_k, x_{k-1}, \dots, x_{k-N}) - \Psi(x_{k+1}, x_k, \dots, x_{k-N+1})) \\ &= \Psi(x_0, x_{-1}, \dots, x_{-N}) - \Psi(x_{K+1}, x_K, \dots, x_{K-N+1}) \\ &\leq \Psi(x_0, x_{-1}, \dots, x_{-N}) - F_{low}, \end{aligned} \quad (46)$$

where the last inequality follows from Assumption 1(iii) and the definition of the merit function  $\Psi$  in (38). The thesis follows by taking the limit for  $K \rightarrow \infty$  on inequality (46) and noting that its right-hand side is independent of  $K$ .  $\square$

To proceed further with the analysis, it is crucial to assume that also  $\phi$  is continuously differentiable with locally Lipschitz continuous gradient. Such a differentiability assumption could be neglected if  $\phi$  was a separable sum with respect to the blocks, i.e., in the case where  $\phi(x) = \sum_{i=1}^N \phi_i(U_i^T x)$ . Assuming that  $\phi$  is a separable sum is quite common in the literature of block-coordinate proximal–gradient methods [9, 12, 19, 22, 25, 34]; however, we prefer to assume the differentiability of  $\phi$  and drop the separability assumption, as the PnP framework based on model (27) does not allow neither  $f$  nor  $\phi$  to be separable.

**Assumption 3.**  $\phi$  is continuously differentiable and  $\nabla\phi$  is locally Lipschitz continuous, i.e., for all compact subsets  $K \subseteq \mathbb{R}^n$  there exists  $L_{\phi,K} > 0$  such that

$$\|\nabla\phi(x) - \nabla\phi(y)\| \leq L_{\phi,K}\|x - y\|, \quad \forall x, y \in K. \quad (47)$$

The following Lemma shows an upper bound on the norm of the gradient of the objective function along the iterates  $\{\hat{u}_k\}_{k \in \mathbb{N}}$ , which are defined so that  $U_{i_k}^T \hat{u}_k = \hat{y}_k$  and  $U_j^T \hat{u}_k = U_j^T x_k$  for any  $j \neq i_k$ . The result is inspired by [18, Lemma 3.2], although unlike in [18] we need to take into account the inexactness of the proximal–gradient point, as well as the presence of inertial terms, variable metrics and a linesearch procedure. As in [18], we require the sequence  $\{x_k\}_{k \in \mathbb{N}}$  to be bounded, which is used in combination with the local Lipschitz continuity of  $\nabla\phi$  to ensure the existence of the upper bound.

**Lemma 4.4.** *Suppose Assumptions 1-2-3 hold and  $\{x_k\}_{k \in \mathbb{N}}$  is a bounded sequence. Set*

$$\hat{u}_k = x_k + U_{i_k}(\hat{y}_k - U_{i_k}^T x_k), \quad \forall k \in \mathbb{N}. \quad (48)$$

Then, for all  $k \geq N$ , there exists  $b > 0$  such that

$$\|\nabla F(\hat{u}_k)\|^2 \leq b^2 \sum_{j=-(N-1)}^N (-h_{k+j-1}(\tilde{y}_{k+j-1})). \quad (49)$$

*Proof.* We start by noting that the sequence  $\{\hat{u}_k\}_{k \in \mathbb{N}}$  is bounded, due to the boundedness of  $\{x_k\}_{k \in \mathbb{N}}$  and the continuity of the proximal operator with respect to its parameters. Then, there exists a compact  $K \subseteq \mathbb{R}^n$  that contains both  $\{x_k\}_{k \in \mathbb{N}}$  and  $\{\hat{u}_k\}_{k \in \mathbb{N}}$  and a corresponding Lipschitz constant  $L_{\phi,K}$  satisfying Assumption 3. As also Assumption 2 holds, we can conclude that the following local, Lipschitz-block conditions are valid for all  $i = 1, \dots, N$ :

$$\|U_i^T(\nabla f(x) - \nabla f(y))\| \leq L_f\|x - y\|, \quad \|U_i^T(\nabla\phi(x) - \nabla\phi(y))\| \leq L_{\phi,K}\|x - y\|, \quad \forall x, y \in K. \quad (50)$$

Furthermore, we recall that the proximal–gradient point  $\hat{y}_k$  is the unique minimum point of the function  $h_k$  defined in (24), i.e.,  $\hat{y}_k = \operatorname{argmin}_{y \in \mathbb{R}^{n_{i_k}}} h_k(y)$ , and the corresponding optimality condition can be rewritten as follows

$$\begin{aligned} \nabla h_k(\hat{y}_k) = 0 &\Leftrightarrow U_{i_k}^T \nabla f(x_k) - \frac{\beta_k}{\alpha_k} D_k U_{i_k}^T (x_k - x_{k-N}) + \frac{1}{\alpha_k} D_k (\hat{y}_k - U_{i_k}^T x_k) + \nabla \phi_{i_k}^{x_k}(\hat{y}_k) = 0 \\ &\Leftrightarrow U_{i_k}^T \nabla \phi(x_k + U_{i_k}(\hat{y}_k - U_{i_k}^T x_k)) \\ &= -U_{i_k}^T \nabla f(x_k) + \frac{\beta_k}{\alpha_k} D_k U_{i_k}^T (x_k - x_{k-N}) - \frac{1}{\alpha_k} D_k (\hat{y}_k - U_{i_k}^T x_k) \\ &\Leftrightarrow U_{i_k}^T \nabla \phi(\hat{u}_k) = -U_{i_k}^T \nabla f(x_k) + \frac{\beta_k}{\alpha_k} D_k U_{i_k}^T (x_k - x_{k-N}) - \frac{1}{\alpha_k} D_k (\hat{y}_k - U_{i_k}^T x_k), \end{aligned} \quad (51)$$

where the second equivalence follows from the definition of  $\phi_{i_k}^{x_k}$  in (21) and the chain rule holding for differentiable functions, whereas the third is obtained by definition of the point  $\hat{u}_k$  in (48).

Based on (51), the quantity  $\|\nabla F(\hat{u}_k)\|^2$  can be rewritten as follows:

$$\begin{aligned}\|\nabla F(\hat{u}_k)\|^2 &= \sum_{j=1}^N \|U_{i_{k+j-1}}^T \nabla F(\hat{u}_k)\|^2 = \sum_{j=1}^N \|U_{i_{k+j-1}}^T (\nabla f(\hat{u}_k) + \nabla \phi(\hat{u}_k))\|^2 \\ &= \sum_{j=1}^N \|U_{i_{k+j-1}}^T (\nabla f(\hat{u}_k) - \nabla f(x_{k+j-1}) + \nabla \phi(\hat{u}_k) - \nabla \phi(\hat{u}_{k+j-1}))\|^2 \\ &\quad - \frac{1}{\alpha_{k+j-1}} \|D_{k+j-1}(\hat{y}_{k+j-1} - U_{i_{k+j-1}}^T x_{k+j-1}) + \frac{\beta_{k+j-1}}{\alpha_{k+j-1}} D_{k+j-1} U_{i_{k+j-1}}^T (x_{k+j-1} - x_{k+j-1-N})\|^2,\end{aligned}$$

where the third equality is due to the optimality condition (51) with  $k$  replaced by  $k+j-1$ . Applying the relation  $\|a+b\|^2 \leq 2\|a\|^2 + 2\|b\|^2$  three times and STEP 2 of Algorithm 1 yields

$$\begin{aligned}\|\nabla F(\hat{u}_k)\|^2 &\leq 4 \sum_{j=1}^N \left( \|U_{i_{k+j-1}}^T (\nabla f(\hat{u}_k) - \nabla f(x_{k+j-1}))\|^2 + \frac{1}{\alpha_{k+j-1}} \|D_{k+j-1}(\hat{y}_{k+j-1} - U_{i_{k+j-1}}^T x_{k+j-1})\|^2 \right) \\ &\quad + 4 \sum_{j=1}^N \left( \|U_{i_{k+j-1}}^T (\nabla \phi(\hat{u}_k) - \nabla \phi(\hat{u}_{k+j-1}))\|^2 + \frac{\beta_{k+j-1}}{\alpha_{k+j-1}} \|D_{k+j-1} U_{i_{k+j-1}}^T (x_{k+j-1} - x_{k+j-1-N})\|^2 \right) \\ &\leq 4 \sum_{j=1}^N \left( \|U_{i_{k+j-1}}^T (\nabla f(\hat{u}_k) - \nabla f(x_{k+j-1}))\|^2 + \frac{\mu}{\alpha_{\min}} \|\hat{y}_{k+j-1} - U_{i_{k+j-1}}^T x_{k+j-1}\|^2 \right) \\ &\quad + 4 \sum_{j=1}^N \left( \|U_{i_{k+j-1}}^T (\nabla \phi(\hat{u}_k) - \nabla \phi(\hat{u}_{k+j-1}))\|^2 + \frac{\beta_{\max} \mu}{\alpha_{\min}} \|U_{i_{k+j-1}}^T (x_{k+j-1} - x_{k+j-1-N})\|^2 \right).\end{aligned}$$

By applying the inequalities in (50), we get

$$\begin{aligned}\|\nabla F(\hat{u}_k)\|^2 &\leq 4L_f^2 \sum_{j=1}^N \|\hat{u}_k - x_{k+j-1}\|^2 + \frac{4\mu}{\alpha_{\min}} \sum_{j=1}^N \|\hat{y}_{k+j-1} - U_{i_{k+j-1}}^T x_{k+j-1}\|^2 \\ &\quad + 4L_{\phi,K}^2 \sum_{j=1}^N \|\hat{u}_k - \hat{u}_{k+j-1}\|^2 + \frac{4\beta_{\max} \mu}{\alpha_{\min}} \sum_{j=1}^N \|U_{i_{k+j-1}}^T (x_{k+j-1} - x_{k+j-1-N})\|^2 \\ &= 4L_f^2 \sum_{j=1}^N \|\hat{u}_k - x_k + \sum_{t=1}^{j-1} (x_{k+t-1} - x_{k+t})\|^2 + \frac{4\mu}{\alpha_{\min}} \sum_{j=1}^N \|\hat{y}_{k+j-1} - U_{i_{k+j-1}}^T x_{k+j-1}\|^2 \\ &\quad + 4L_{\phi,K}^2 \sum_{j=1}^N \|\hat{u}_k - x_k + \sum_{t=1}^{j-1} (x_{k+t-1} - x_{k+t}) + x_{k+j-1} - \hat{u}_{k+j-1}\|^2 \\ &\quad + \frac{4\beta_{\max} \mu}{\alpha_{\min}} \sum_{j=1}^N \|U_{i_{k+j-1}}^T (x_{k+j-1} - x_{k+j-1-N})\|^2.\end{aligned}$$

Repeatedly applying Jensen's inequality to the above inequality yields

$$\begin{aligned}
\|\nabla F(\hat{u}_k)\|^2 &\leq 4L_f^2 \sum_{j=1}^N \left( 2\|\hat{u}_k - x_k\|^2 + 2(j-1) \sum_{t=1}^{j-1} \|x_{k+t-1} - x_{k+t}\|^2 \right) \\
&\quad + 4L_{\phi,K}^2 \sum_{j=1}^N \left( 2\|\hat{u}_k - x_k\|^2 + 4\|x_{k+j-1} - \hat{u}_{k+j-1}\|^2 + 4(j-1) \sum_{t=1}^{j-1} \|x_{k+t-1} - x_{k+t}\|^2 \right) \\
&\quad + \frac{4\mu}{\alpha_{\min}} \sum_{j=1}^N \|\hat{y}_{k+j-1} - U_{i_{k+j-1}}^T x_{k+j-1}\|^2 + \frac{4\beta_{\max}\mu}{\alpha_{\min}} \sum_{j=1}^N \|U_{i_{k+j-1}}^T (x_{k+j-1} - x_{k+j-1-N})\|^2.
\end{aligned} \tag{52}$$

Next, we upper-bound some of the squared norms appearing in (52). We note that

$$\|\hat{u}_k - x_k\| = \|U_{i_k}(\hat{y}_k - U_{i_k}^T x_k)\| = \|\hat{y}_k - U_{i_k}^T x_k\| \tag{53}$$

$$\|\hat{u}_{k+j-1} - x_{k+j-1}\| = \|\hat{y}_{k+j-1} - U_{i_{k+j-1}}^T x_{k+j-1}\|. \tag{54}$$

Furthermore, by STEP 6 of Algorithm 1, it is either  $x_{k+t} - x_{k+t-1} = \lambda_{k+t-1} U_{i_{k+t-1}} d_{k+t-1}$  or  $x_{k+t} - x_{k+t-1} = U_{i_{k+t-1}} d_{k+t-1}$ , so that in both cases

$$\|x_{k+t} - x_{k+t-1}\| \leq \|U_{i_{k+t-1}} d_{k+t-1}\| = \|d_{k+t-1}\|. \tag{55}$$

In addition, following a similar reasoning as in (41), we can show that

$$\begin{aligned}
\|U_{i_{k+j-1}}^T (x_{k+j-1} - x_{k+j-1-N})\| &= \|U_{i_{k+j-1}}^T (x_{k+j-N} - x_{k+j-1-N})\| \\
&= \|x_{k+j-N} - x_{k+j-N-1}\| \leq \|d_{k+j-N-1}\|.
\end{aligned} \tag{56}$$

Plugging (53)-(54)-(55)-(56) into (52) yields

$$\begin{aligned}
\|\nabla F(\hat{u}_k)\|^2 &\leq 4L_f^2 \sum_{j=1}^N \left( 2\|\hat{y}_k - U_{i_k}^T x_k\|^2 + 2(N-1) \sum_{t=1}^N \|d_{k+t-1}\|^2 \right) \\
&\quad + 4L_{\phi,K}^2 \sum_{j=1}^N \left( 2\|\hat{y}_k - U_{i_k}^T x_k\|^2 + 4\|\hat{y}_{k+j-1} - U_{i_{k+j-1}}^T x_{k+j-1}\|^2 + 4(N-1) \sum_{t=1}^N \|d_{k+t-1}\|^2 \right) \\
&\quad + \frac{4\mu}{\alpha_{\min}} \sum_{j=1}^N \|\hat{y}_{k+j-1} - U_{i_{k+j-1}}^T x_{k+j-1}\|^2 + \frac{4\beta_{\max}\mu}{\alpha_{\min}} \sum_{j=1}^N \|d_{k+j-N-1}\|^2 \\
&= 8N(N-1)(L_f^2 + 2L_{\phi,K}^2) \sum_{t=1}^N \|d_{k+t-1}\|^2 + 4 \left( \frac{\mu}{\alpha_{\min}} + 4L_{\phi,K}^2 \right) \sum_{j=1}^N \|\hat{y}_{k+j-1} - U_{i_{k+j-1}}^T x_{k+j-1}\|^2 \\
&\quad + 8N(L_f^2 + L_{\phi,K}^2) \|\hat{y}_k - U_{i_k}^T x_k\|^2 + \frac{4\beta_{\max}\mu}{\alpha_{\min}} \sum_{j=1}^N \|d_{k+j-N-1}\|^2.
\end{aligned}$$

Now, we can apply Lemma 4.1 to all the squared norms in the previous inequality, thus concluding there exist  $b_1 > 0$  and  $b_2 > 0$  such that

$$\|\nabla F(\hat{u}_k)\|^2 \leq b_1^2 \sum_{j=1}^N (-h_{k+j-1}(\tilde{y}_{k+j-1})) + b_2^2 \sum_{j=1}^N (-h_{k+j-N-1}(\tilde{y}_{k+j-N-1})).$$

Finally, the thesis follows by setting  $b = \sqrt{\max\{b_1^2, b_2^2\}}$ .  $\square$

Thanks to the previous Lemma, it is possible to prove the first mild convergence result for Algorithm 1, as detailed in the following Theorem.

**Theorem 4.5.** *Suppose Assumptions 1-2-3 hold and  $\{x_k\}_{k \in \mathbb{N}}$  is a bounded sequence. The following statements hold true.*

(i) *We have  $\sum_{k=0}^{\infty} \|\nabla F(x_k)\|^2 < \infty$ , thus each limit point of  $\{x_k\}_{k \in \mathbb{N}}$  is stationary for  $F$ .*

(ii) *There exists  $C > 0$  such that*

$$\min_{0 \leq i \leq K} \|\nabla F(x_i)\|^2 \leq \frac{C}{K+1}.$$

*Proof.* (i) Let  $K \geq N$ . We sum inequality (49) for  $k = N, N+1, \dots, K$ , so as to obtain

$$\begin{aligned} \sum_{k=N}^K \|\nabla F(\hat{u}_k)\|^2 &\leq \sum_{k=N}^K \left( b^2 \sum_{j=-(N-1)}^N (-h_{k+j-1}(\tilde{y}_{k+j-1})) \right) = b^2 \sum_{j=-(N-1)}^N \left( \sum_{k=N}^K (-h_{k+j-1}(\tilde{y}_{k+j-1})) \right) \\ &= b^2 \sum_{j=-(N-1)}^N \sum_{k'=N+j-1}^{K+j-1} (-h_{k'}(\tilde{y}_{k'})) \\ &\leq 2b^2 N \sum_{k'=0}^{K+N-1} (-h_{k'}(\tilde{y}_{k'})). \end{aligned} \quad (57)$$

By taking the limit for  $K \rightarrow \infty$  on both sides of (57) and exploiting property (40), we get

$$\sum_{k=0}^{\infty} \|\nabla F(\hat{u}_k)\|^2 < \infty. \quad (58)$$

In order to conclude, we observe that

$$\begin{aligned} \|\nabla F(x_k)\|^2 &\leq 2\|\nabla F(x_k) - \nabla F(\hat{u}_k)\|^2 + 2\|\nabla F(\hat{u}_k)\|^2 \\ &= 2 \left\| \sum_{i=1}^N U_i^T (\nabla F(x_k) - \nabla F(x_k + U_{i_k}(\hat{y}_k - U_{i_k}^T x_k))) \right\|^2 + 2\|\nabla F(\hat{u}_k)\|^2 \\ &\leq 2N \sum_{i=1}^N \left\| U_i^T (\nabla F(x_k) - \nabla F(x_k + U_{i_k}(\hat{y}_k - U_{i_k}^T x_k))) \right\|^2 + 2\|\nabla F(\hat{u}_k)\|^2 \\ &\leq 2N^2 L_f^2 \|\hat{y}_k - U_{i_k}^T x_k\|^2 + 2\|\nabla F(\hat{u}_k)\|^2 \\ &\leq 4N^2 L_f^2 \alpha_{\max} \mu \left( 1 + \frac{\tau}{2} \right) (-h_k(\tilde{y}_k)) + 2\|\nabla F(\hat{u}_k)\|^2, \end{aligned} \quad (59)$$

where the first two inequalities follow by using Jensen's inequality, the third is due to property (50), and the fourth is implied by inequality (34). Summing (59) for  $k = 0, \dots, K$  leads to

$$\sum_{k=0}^K \|\nabla F(x_k)\|^2 \leq 4N^2 L_f^2 \alpha_{\max} \mu \left( 1 + \frac{\tau}{2} \right) \sum_{k=0}^K (-h_k(\tilde{y}_k)) + 2 \sum_{k=0}^K \|\nabla F(\hat{u}_k)\|^2. \quad (60)$$

By taking the limit of (60) for  $K \rightarrow \infty$ , and applying (58) and item (i), we get that  $\{\|\nabla F(x_k)\|^2\}_{k \in \mathbb{N}}$  is summable. Hence, the limit  $\lim_{k \rightarrow \infty} \|\nabla F(x_k)\| = 0$  holds, and by continuity of  $\nabla F$ , we conclude that each limit point is stationary.

(ii) We bound the finite sums in the right-hand side of (60) with their (finite) limits to obtain

$$\sum_{k=0}^K \|\nabla F(x_k)\|^2 \leq 4N^2 L_f^2 \alpha_{\max} \mu \left( 1 + \frac{\tau}{2} \right) \sum_{k=0}^{\infty} (-h_k(\tilde{y}_k)) + 2 \sum_{k=0}^{\infty} \|\nabla F(\hat{u}_k)\|^2 < \infty.$$

The thesis then follows by applying the definition of minimum to the above inequality.  $\square$

## 4.2 Convergence under the KL property

In the following, we are interested in proving the convergence of the sequence  $\{x_k\}_{k \in \mathbb{N}}$  generated by Algorithm 1 to a stationary point of  $F$ . To this aim, we rely on the following abstract convergence result.

**Theorem 4.6.** [13, Theorem 14] *Let  $\mathcal{F} : \mathbb{R}^n \times \mathbb{R}^m \rightarrow \bar{\mathbb{R}}$  be a proper, lower semicontinuous KL function and  $\Psi : \mathbb{R}^n \times \mathbb{R}^q \rightarrow \bar{\mathbb{R}}$  a proper, lower semicontinuous function that is bounded from below. Consider a sequence  $\{(x_k, \rho_k)\}_{k \in \mathbb{N}} \subset \mathbb{R}^n \times \mathbb{R}^m$  such that  $\{x_k\}_{k \in \mathbb{N}}$  is bounded and  $\{\rho_k\}_{k \in \mathbb{N}}$  converges, and let  $\{u_k\}_{k \in \mathbb{N}} \subset \mathbb{R}^n$ ,  $\{r_k\}_{k \in \mathbb{N}} \subset \mathbb{R}^q$ ,  $\{s_k\}_{k \in \mathbb{N}} \subset \mathbb{R}^q$  be chosen such that the following properties hold.*

(i) *There exists a positive real number  $a$  such that*

$$\Psi(x_{k+1}, s_{k+1}) + ar_k^2 \leq \Psi(x_k, s_k), \quad \forall k \in \mathbb{N}. \quad (61)$$

(ii) *There exists a sequence of non-negative real numbers  $\{t_k\}_{k \in \mathbb{N}}$  with  $\lim_{k \rightarrow \infty} t_k = 0$  such that*

$$\Psi(x_{k+1}, s_{k+1}) \leq \mathcal{F}(u_k, \rho_k) \leq \Psi(x_k, s_k) + t_k, \quad \forall k \in \mathbb{N}. \quad (62)$$

(iii) *There exists a subgradient  $w_k \in \partial \mathcal{F}(u_k, \rho_k)$  such that*

$$\|w_k\| \leq p \sum_{i \in \mathcal{I}} r_{k+1-i}, \quad \forall k \in \mathbb{N}, \quad (63)$$

where  $p$  is a positive real number,  $\mathcal{I} \subset \mathbb{Z}$  is a non-empty, finite index set, and  $r_j = 0$  for  $j \leq 0$ .

(iv) *If  $\{(x_{k_j}, \rho_{k_j})\}_{j \in \mathbb{N}}$  is a subsequence of  $\{(x_k, \rho_k)\}_{k \in \mathbb{N}}$  converging to some  $(x^*, \rho^*) \in \mathbb{R}^n \times \mathbb{R}^m$ , then we have*

$$\lim_{j \rightarrow \infty} \|u_{k_j} - x_{k_j}\| = 0, \quad \lim_{j \rightarrow \infty} \mathcal{F}(u_{k_j}, \rho_{k_j}) = \mathcal{F}(x^*, \rho^*). \quad (64)$$

(v) *There exists a positive real number  $q > 0$  such that*

$$\|x_{k+1} - x_k\| \leq qr_k, \quad \forall k \in \mathbb{N}. \quad (65)$$

Then, the sequence  $\{(x_k, \rho_k)\}_{k \in \mathbb{N}}$  converges to a stationary point of  $\mathcal{F}$ .

Theorem 4.6 guarantees the convergence of the abstract iterates  $\{(x_k, \rho_k)\}_{k \in \mathbb{N}}$  to a stationary point of the KL function  $\mathcal{F}$ , provided that the iterates comply with properties (61)-(65). Such a result generalizes several abstract convergence results holding under the KL inequality and similar assumptions on the iterates [5, 9, 34]. By relying on Theorem 4.6, we can ensure the convergence of the iterates generated by Algorithm 1 to a stationary point of  $F$ . To this aim, the role of the merit function  $\Psi$  appearing in Theorem 4.6 is played by the function in (38), whereas the other merit function  $\mathcal{F}$  is defined as

$$\mathcal{F}(x, \rho) = F(x) + \frac{1}{2}\rho^2, \quad \forall (x, \rho) \in \mathbb{R}^n \times \mathbb{R}. \quad (66)$$

Note that the function (66) is a KL function whenever  $F$  is definable in an  $o$ -minimal structure [8, Definition 6], as definable functions do satisfy the KL inequality on their domains and finite sums of definable functions in some  $o$ -minimal structure remain in the same structure [8, Remark 5]. When the specific PnP model (27) is considered, we can ensure  $F$  is definable whenever the data fidelity  $\phi$  and the regularizer  $g_\sigma$  in (3) are definable in the same structure. Interestingly, if  $\phi$  is chosen as a least-squares functional, then  $g_\sigma$  is definable in the same structure as  $\phi$  provided that the employed neural network  $N_\sigma$  is built upon definable functions such as ReLU, eLU, quadratics and SoftPlus functions, as the composition of definable functions remains definable [21, Section 5.2]. This is exactly the scenario addressed in our numerical experiments, where  $\phi(x) = \frac{1}{2}\|Ax - b\|^2$  with  $b \in \mathbb{R}^n$ ,  $A \in \mathbb{R}^{m \times n}$ , and the neural network used in  $g_\sigma$  is defined by means of linear and eLU functions (see Section 5).

We now state the convergence result holding for Algorithm 1 and based on Theorem 4.6.

**Corollary 4.1.** *Suppose Assumptions 1-2-3 hold. If the sequence  $\{x_k\}_{k \in \mathbb{N}}$  generated by Algorithm 1 is bounded and the function  $\mathcal{F}$  defined in (66) is a KL function, then  $\{x_k\}_{k \in \mathbb{N}}$  converges to a stationary point of  $F$ .*

*Proof.* The proof consists in showing that Algorithm 1 satisfies the properties from (61) to (65) enlisted in Theorem 4.6.

According to Lemma 4.3, we immediately obtain the descent property (61) with  $\Psi$  defined as in (38),  $r_k = \sqrt{-h_k(\tilde{y}_k)}$ ,  $s_k = (x_{k-1}, \dots, x_{k-N})$  and  $a = \lambda_{\min} \sigma$ .

Next, we show that property (62) holds. As noted in the proof of Lemma 4.4, the sequence  $\{\hat{u}_k\}_{k \in \mathbb{N}}$  defined in (48) is bounded. Furthermore, let  $\tilde{u}_k = x_k + U_{i_k} d_k$  for all  $k \in \mathbb{N}$ . From inequalities (36) and (40), it follows that  $\lim_{k \rightarrow \infty} d_k = 0$ ; by combining this limit with the boundedness of  $\{x_k\}_{k \in \mathbb{N}}$ , we conclude that also  $\{\tilde{u}_k\}_{k \in \mathbb{N}}$  is bounded. Now, let  $\tilde{K} \subseteq \mathbb{R}^n$  be any compact set containing both  $\{\hat{u}_k\}_{k \in \mathbb{N}}$  and  $\{\tilde{u}_k\}_{k \in \mathbb{N}}$ . Since  $\nabla F$  is locally Lipschitz continuous by Assumptions 2 and 3, the Descent Lemma for  $F$  locally holds on  $\tilde{K}$  [6, Lemma 5.7], i.e., there exists  $L_{F, \tilde{K}} > 0$  such that

$$F(y) \leq F(x) + \nabla F(x)^T (y - x) + \frac{L_{F, \tilde{K}}}{2} \|y - x\|^2, \quad \forall x, y \in \tilde{K}. \quad (67)$$

By setting  $x = \hat{u}_k$  and  $y = \tilde{u}_k$  in equation (67), we obtain

$$\begin{aligned} F(\tilde{u}_k) &\leq F(\hat{u}_k) + \nabla F(\hat{u}_k)^T (\tilde{u}_k - \hat{u}_k) + \frac{L_{F, \tilde{K}}}{2} \|\tilde{u}_k - \hat{u}_k\|^2 \\ &= F(\hat{u}_k) + (U_{i_k}^T \nabla F(\hat{u}_k))^T (\tilde{y}_k - \hat{y}_k) + \frac{L_{F, \tilde{K}}}{2} \|\tilde{y}_k - \hat{y}_k\|^2. \end{aligned} \quad (68)$$

By summing the term  $U_{i_k}^T \nabla f(\hat{u}_k)$  to both sides of (51), we can express the  $i_k$ -block of coordinates of  $\nabla F(\hat{u}_k)$  through the following equality

$$U_{i_k}^T \nabla F(\hat{u}_k) = U_{i_k}^T (\nabla f(\hat{u}_k) - \nabla f(x_k)) + \frac{\beta_k}{\alpha_k} D_k U_{i_k}^T (x_k - x_{k-N}) - \frac{1}{\alpha_k} D_k (\hat{y}_k - U_{i_k}^T x_k). \quad (69)$$

Plugging (69) in (68) yields

$$\begin{aligned} F(\tilde{u}_k) &\leq F(\hat{u}_k) + (\nabla f(\hat{u}_k) - \nabla f(x_k))^T U_{i_k} (\tilde{y}_k - \hat{y}_k) + \frac{L_{F, \tilde{K}}}{2} \|\tilde{y}_k - \hat{y}_k\|^2 \\ &\quad + \frac{\beta_k}{\alpha_k} (x_k - x_{k-N})^T U_{i_k} D_k (\tilde{y}_k - \hat{y}_k) - \frac{1}{\alpha_k} (\hat{y}_k - U_{i_k}^T x_k)^T D_k (\tilde{y}_k - \hat{y}_k) \\ &\leq F(\hat{u}_k) + L_f \|\hat{u}_k - x_k\| \|\tilde{y}_k - \hat{y}_k\| + \frac{L_{F, \tilde{K}}}{2} \|\tilde{y}_k - \hat{y}_k\|^2 \\ &\quad + \frac{\beta_k}{\alpha_k} \|U_{i_k}^T (x_k - x_{k-N})\| \|D_k (\tilde{y}_k - \hat{y}_k)\| + \frac{1}{\alpha_k} \|\hat{y}_k - U_{i_k}^T x_k\| \|D_k (\tilde{y}_k - \hat{y}_k)\| \\ &\leq F(\hat{u}_k) + \left( L_f + \frac{\mu}{\alpha_{\min}} \right) \|\hat{y}_k - U_{i_k}^T x_k\| \|\tilde{y}_k - \hat{y}_k\| + \frac{L_{F, \tilde{K}}}{2} \|\tilde{y}_k - \hat{y}_k\|^2 \\ &\quad + \frac{\beta_{\max} \mu}{\alpha_{\min}} \|\tilde{y}_k - \hat{y}_k\| \|x_{k-N+1} - x_{k-N}\|, \end{aligned}$$

where the second inequality follows by applying the Cauchy-Schwarz inequality and the Lipschitz continuity of  $\nabla f$ , and the third is due to the definition of  $\hat{u}_k$  in (48), STEP 2 of Algorithm 1, and equality (41). We now sum the term  $\frac{\gamma}{2} \|d_k\|^2 + \frac{\gamma}{2} \sum_{i=1}^{N-1} \|x_{k-i+1} - x_{k-i}\|^2$  to both sides of the obtained

inequality and recall the definition of the function  $\Psi$  in (38), hence obtaining

$$\begin{aligned}
\Psi(\tilde{u}_k, x_k, \dots, x_{k-N+1}) &\leq F(\hat{u}_k) + \frac{\gamma}{2} \|d_k\|^2 + \frac{\gamma}{2} \sum_{i=1}^{N-1} \|x_{k-i+1} - x_{k-i}\|^2 \\
&\quad + \frac{L_{F,\tilde{K}}}{2} \|\tilde{y}_k - \hat{y}_k\|^2 + \left( L_f + \frac{\mu}{\alpha_{\min}} \right) \|\hat{y}_k - U_{i_k}^T x_k\| \|\tilde{y}_k - \hat{y}_k\| \\
&\quad + \frac{\beta_{\max} \mu}{\alpha_{\min}} \|\tilde{y}_k - \hat{y}_k\| \|x_{k-N+1} - x_{k-N}\| \\
&\leq F(\hat{u}_k) + \frac{\gamma}{2} \|d_k\|^2 + \frac{\gamma}{2} \sum_{i=1}^{N-1} \|d_{k-i}\|^2 + \frac{L_{F,\tilde{K}}}{2} \|\tilde{y}_k - \hat{y}_k\|^2 \\
&\quad + \left( L_f + \frac{\mu}{\alpha_{\min}} \right) \|\hat{y}_k - U_{i_k}^T x_k\| \|\tilde{y}_k - \hat{y}_k\| + \frac{\beta_{\max} \mu}{\alpha_{\min}} \|\tilde{y}_k - \hat{y}_k\| \|d_{k-N}\|, \quad (70)
\end{aligned}$$

where each norm  $\|x_{k-i+1} - x_{k-i}\|$  has been bounded with  $\|d_{k-i}\|$  thanks to inequality (55). Thus, we define  $\{\rho_k\}_{k \in \mathbb{N}}$  as the nonnegative sequence such that

$$\begin{aligned}
\frac{\rho_k^2}{2} &= \frac{\gamma}{2} \|d_k\|^2 + \frac{\gamma}{2} \sum_{i=1}^{N-1} \|d_{k-i}\|^2 + \frac{L_{F,\tilde{K}}}{2} \|\tilde{y}_k - \hat{y}_k\|^2 \\
&\quad + \left( L_f + \frac{\mu}{\alpha_{\min}} \right) \|\hat{y}_k - U_{i_k}^T x_k\| \|\tilde{y}_k - \hat{y}_k\| + \frac{\beta_{\max} \mu}{\alpha_{\min}} \|\tilde{y}_k - \hat{y}_k\| \|d_{k-N}\|. \quad (71)
\end{aligned}$$

Recalling the definition of  $\mathcal{F}$  in (66) and using (71) in (70) leads to

$$\Psi(\tilde{u}_k, x_k, x_{k-1}, \dots, x_{k-N+1}) \leq \mathcal{F}(\hat{u}_k, \rho_k). \quad (72)$$

By using (43) and the definition of  $\tilde{u}_k$ , it immediately follows that

$$\Psi(x_{k+1}, x_k, x_{k-1}, \dots, x_{k-N+1}) \leq \Psi(\tilde{u}_k, x_k, x_{k-1}, \dots, x_{k-N+1}) \leq \mathcal{F}(\hat{u}_k, \rho_k), \quad (73)$$

which is exactly the left-hand inequality of property (62) with  $u_k = \hat{u}_k$ . Furthermore, if we replace  $F$  with  $f$  and  $L_{F,\tilde{K}}$  with  $L_f$  in the Descent Lemma (67) and set  $y = \hat{u}_k$  and  $x = x_k$ , we can write

$$\begin{aligned}
f(\hat{u}_k) &\leq f(x_k) + \nabla f(x_k)^T (\hat{u}_k - x_k) + \frac{L_f}{2} \|\hat{u}_k - x_k\|^2 \\
&= f(x_k) + (U_{i_k}^T \nabla f(x_k))^T (\hat{y}_k - U_{i_k}^T x_k) + \frac{L_f}{2} \|\hat{y}_k - U_{i_k}^T x_k\|^2.
\end{aligned}$$

By summing the term  $\phi(\hat{u}_k)$  to both sides of the above inequality, and observing that  $\phi(\hat{u}_k) = \phi_{i_k}^{x_k}(\hat{y}_k)$  and  $\phi(x_k) = \phi_{i_k}^{x_k}(U_{i_k}^T x_k)$  (see (21)), the following inequalities hold

$$\begin{aligned}
F(\hat{u}_k) &\leq F(x_k) + (U_{i_k}^T \nabla f(x_k))^T (\hat{y}_k - U_{i_k}^T x_k) + \phi_{i_k}^{x_k}(\hat{y}_k) - \phi_{i_k}^{x_k}(U_{i_k}^T x_k) + \frac{L_f}{2} \|\hat{y}_k - U_{i_k}^T x_k\|^2 \\
&\leq F(x_k) + h_k(\hat{y}_k) + \frac{L_f}{2} \|\hat{y}_k - U_{i_k}^T x_k\|^2 + \frac{\beta_k}{\alpha_k} (x_k - x_{k-N})^T U_{i_k} D_k (\hat{y}_k - U_{i_k}^T x_k) \\
&\leq F(x_k) + h_k(\hat{y}_k) + \frac{L_f}{2} \|\hat{y}_k - U_{i_k}^T x_k\|^2 + \frac{\beta_{\max} \mu}{\alpha_{\min}} \|x_{k-N+1} - x_{k-N}\| \|\hat{y}_k - U_{i_k}^T x_k\| \\
&\leq F(x_k) + \frac{L_f}{2} \|\hat{y}_k - U_{i_k}^T x_k\|^2 + \frac{\beta_{\max} \mu}{\alpha_{\min}} \|d_{k-N}\| \|\hat{y}_k - U_{i_k}^T x_k\|, \quad (74)
\end{aligned}$$

where the second inequality is obtained by adding the term  $\frac{1}{2\alpha_k} \|\hat{y}_k - U_{i_k}^T x_k\|_{D_k}^2$ , summing and subtracting the term  $\langle \frac{\beta_k}{\alpha_k} D_k U_{i_k}^T (x_k - x_{k-N}), \hat{y}_k - U_{i_k}^T x_k \rangle$  and recalling the definition of  $h_k$  in (24), the

third follows by applying the Cauchy-Schwarz inequality, STEP 2 of Algorithm 1 and equality (41), and the fourth is due to  $h_k(\hat{y}_k) \leq h_k(U_{i_k}^T x_k) = 0$  and (55). We sum the term  $\rho_k^2/2$  to both sides of (74) and observe that  $F(x_k) \leq \Psi(x_k, x_{k-1}, \dots, x_{k-N})$  by definition of  $\Psi$  in (38), so as to obtain

$$\mathcal{F}(\hat{u}_k, \rho_k) \leq \Psi(x_k, x_{k-1}, \dots, x_{k-N}) + \frac{L_f}{2} \|\hat{y}_k - U_{i_k}^T x_k\|^2 + \frac{\beta_{\max} \mu}{\alpha_{\min}} \|d_{k-N}\| \|\hat{y}_k - U_{i_k}^T x_k\| + \frac{\rho_k^2}{2}.$$

At this point, we conveniently define the sequence  $\{t_k\}_{k \in \mathbb{N}}$  as

$$t_k = \frac{L_f}{2} \|\hat{y}_k - U_{i_k}^T x_k\|^2 + \frac{\beta_{\max} \mu}{\alpha_{\min}} \|d_{k-N}\| \|\hat{y}_k - U_{i_k}^T x_k\| + \frac{\rho_k^2}{2}. \quad (75)$$

Note that from (71), Lemma 4.1 and the property  $\lim_{k \rightarrow \infty} h_k(\tilde{y}_k) = 0$  (due to (40)), it follows that

$$\lim_{k \rightarrow \infty} \rho_k = 0. \quad (76)$$

Based on (75), (76) and Lemma 4.1, we also obtain that  $\lim_{k \rightarrow \infty} t_k = 0$ , and the right-hand inequality of property (62) is finally proved.

We move on to property (63). By applying Lemma 4.4 and relation  $\sqrt{u+v} \leq \sqrt{u} + \sqrt{v}$ , we have

$$\|\nabla \mathcal{F}(\hat{u}_k, \rho_k)\| \leq \|\nabla F(\hat{u}_k)\| + \rho_k \leq b \sum_{j=-(N-1)}^N \sqrt{-h_{k+j-1}(\tilde{y}_{k+j-1})} + \rho_k.$$

From the definition of  $\rho_k$  in (71) and Lemma 4.1, it is easy to prove the existence of  $b_\rho > 0$  such that

$$\rho_k \leq b_\rho \sum_{j=-(N-1)}^N \sqrt{-h_{k+j-1}(\tilde{y}_{k+j-1})}.$$

Then, property (63) follows by setting  $p = b + b_\rho$  and  $\mathcal{I} = \{-N + 2, \dots, N + 1\}$ .

Property (64) is obtained as follows. From Lemma 4.1, we have that  $\|\hat{u}_k - x_k\| = \|\hat{y}_k - U_{i_k}^T x_k\| \leq \sqrt{2\alpha_{\max} \mu (1 + \frac{\tau}{2}) (-h_k(\tilde{y}_k))}$ ; since equation (40) implies  $\lim_{k \rightarrow \infty} h_k(\tilde{y}_k) = 0$ , it must be  $\lim_{k \rightarrow \infty} \|\hat{u}_k - x_k\| = 0$  and the first limit in (64) holds. The second limit in (64) trivially follows by continuity of the function  $\mathcal{F}$ .

As for property (65), it suffices to note that

$$\|x_{k+1} - x_k\| \leq \|d_k\| \leq \sqrt{2\alpha_{\max} \mu} \left( \sqrt{1 + \frac{\tau}{2}} + \sqrt{\frac{\tau}{2}} \right) \sqrt{-h_k(\tilde{y}_k)},$$

which follows by STEP 6 of Algorithm 1 and Lemma 4.1, and set  $q = \sqrt{2\alpha_{\max} \mu} (\sqrt{1 + \frac{\tau}{2}} + \sqrt{\frac{\tau}{2}})$ .

Since properties from (61) to (65) hold,  $\{x_k\}_{k \in \mathbb{N}}$  is bounded by assumption, and  $\{\rho_k\}_{k \in \mathbb{N}}$  converges as concluded in (76), the assumptions of Theorem 4.6 hold, and thus the iterates  $\{(x_k, \rho_k)\}_{k \in \mathbb{N}}$  converge to a stationary point  $(x^*, 0) \in \mathbb{R}^n \times \mathbb{R}$  of  $\mathcal{F}$ . Since  $\nabla \mathcal{F}(x, \rho) = (\nabla F(x), \rho)$  for all  $(x, \rho) \in \mathbb{R}^n \times \mathbb{R}$ , it follows that the limit point  $x^*$  of  $\{x_k\}_{k \in \mathbb{N}}$  must be stationary for  $F$ , and hence the proof is complete.  $\square$

In the following, we are interested in deriving convergence rates on the function values along the iterates, by assuming that the merit function  $\Psi$  defined in (38) satisfies the KL property at the limit point with  $\phi(t) = ct^{1-\theta}$ , being  $c > 0$  and  $\theta \in [0, 1)$  depending on the point of interest. This type of result is quite common in the KL literature, see e.g. [18, 19, 22].

Our analysis relies on the following Lemma, which contains convergence rates for a non-negative non-increasing sequence complying with a certain recurrence relation. Such a result is similar to [33, Lemma 8], which regards any positive decreasing sequence  $\{\Delta_k\}_{k \in \mathbb{N}}$  satisfying  $\Delta_k^{1+\zeta} \leq \tilde{c}(\Delta_k - \Delta_{k+1})$  with  $\tilde{c} > 0$ ,  $\zeta > -1$ . In our result, we replace  $\Delta_k - \Delta_{k+1}$  with  $\Delta_{k-1} - \Delta_{k+1}$ , which is needed to take into account the presence of an inertial term in Algorithm 1.

**Lemma 4.7.** Let  $\{\Delta_k\}_{k \in \mathbb{N}} \subseteq \mathbb{R}$  be a non-negative, monotone non-increasing sequence such that  $\lim_{k \rightarrow \infty} \Delta_k = 0$ . Suppose there exist  $\theta \in (0, 1)$  and  $\tilde{c} > 0$  such that the following inequality holds:

$$\Delta_{k+1}^{2\theta} \leq \tilde{c}(\Delta_{k-1} - \Delta_{k+1}), \quad \forall k \in \mathbb{N}. \quad (77)$$

Then, the following statements hold true.

(i) If  $\theta \in (\frac{1}{2}, 1)$ , there exists  $C > 0$  such that, for all  $k \in \mathbb{N}$ , we have

$$\Delta_k \leq Ck^{-\frac{1}{2\theta-1}}.$$

(ii) If  $\theta \in (0, \frac{1}{2}]$ , there exists  $C > 0$ ,  $\omega \in (0, 1)$  such that, for all  $k \in \mathbb{N}$ , we have

$$\Delta_k \leq C\omega^k.$$

*Proof.* See Appendix A. □

The convergence rates under the KL assumption on  $\Psi$  are stated in the following Theorem.

**Theorem 4.8.** Suppose the assumptions of Corollary 4.1 are satisfied and let  $x^* \in \mathbb{R}^n$  be the unique limit point of the sequence  $\{x_k\}_{k \in \mathbb{N}}$  generated by Algorithm 1. Assume that the function  $\Psi : \mathbb{R}^n \times \dots \times \mathbb{R}^n \rightarrow \mathbb{R}$  defined in (38) satisfies the KL property at  $(x^*, \dots, x^*)$  with  $\xi(t) = ct^{1-\theta}$ , with  $c > 0$ ,  $\theta \in [0, 1)$ . Then the following convergence rates hold.

(i) If  $\theta = 0$ , the sequence  $\{x_k\}_{k \in \mathbb{N}}$  terminates in a finite number of iterations.

(ii) If  $\theta \in (0, \frac{1}{2}]$ , there exist  $C > 0$ ,  $\omega \in (0, 1)$  such that

$$F(x_{kN}) - F(x^*) \leq C\omega^k. \quad (78)$$

(iii) If  $\theta \in (\frac{1}{2}, 1)$ , there exists  $C > 0$  such that

$$F(x_{kN}) - F(x^*) \leq Ck^{-\frac{1}{2\theta-1}}. \quad (79)$$

*Proof.* Regarding item (i), we assume by contradiction that there exists an infinite subset of indices  $\{k_j\}_{j \in \mathbb{N}}$  such that  $x_{k_j+1} \neq x_{k_j}$  for all  $j \in \mathbb{N}$ . From property (65), we have that  $r_{k_j} > 0$  for all  $j \in \mathbb{N}$ . Since  $\lim_{k \rightarrow \infty} (-h_k(\tilde{y}_k)) = 0$  due to (40), it follows by (34) that  $\lim_{k \rightarrow \infty} \|\hat{u}_k - x_k\| = \lim_{k \rightarrow \infty} \|\hat{y}_k - U_{i_k}^T x_k\| = 0$ . Then, since Corollary 4.1 guarantees that  $\lim_{k \rightarrow \infty} x_k = x^*$ , we have  $\lim_{k \rightarrow \infty} \hat{u}_k = x^*$ . Let  $U$  and  $\nu$  be such that Definition 2.4 is satisfied for the function  $\mathcal{F}$  defined in (66) at the point  $(x^*, 0)$ . Since  $\{\hat{u}_k\}_{k \in \mathbb{N}}$  is converging to  $x^*$ ,  $\{\rho_k\}_{k \in \mathbb{N}}$  is converging to zero and  $\mathcal{F}(\hat{u}_{k_j}, \rho_{k_j}) > \mathcal{F}(x^*, 0)$  thanks to (73), we have  $(\hat{u}_{k_j}, \rho_{k_j}) \in U \cap \{(x, \rho) \in \mathbb{R}^n \times \mathbb{R} : \mathcal{F}(x^*, 0) < \mathcal{F}(x, \rho) < \mathcal{F}(x^*, 0) + \nu\}$  for all sufficiently large  $j \in \mathbb{N}$ . By an abuse of notation, we assume such an inclusion holds for all  $j \in \mathbb{N}$ . Then, the KL inequality can be evaluated at the point  $(\hat{u}_{k_j}, \rho_{k_j})$ , namely

$$\|\nabla \mathcal{F}(\hat{u}_{k_j}, \rho_{k_j})\| \geq \frac{1}{\xi'(\mathcal{F}(\hat{u}_{k_j}, \rho_{k_j}) - \mathcal{F}(x^*, 0))} = \frac{1}{c}, \quad \forall j \in \mathbb{N}, \quad (80)$$

where the equality follows from  $\xi(t) = ct^{1-\theta} = ct$ . By combining (80) and property (63), we obtain

$$\sum_{i \in \mathcal{I}} r_{k_j+1-i} \geq \frac{1}{pc}, \quad \forall j \in \mathbb{N}. \quad (81)$$

Squaring both sides of equation (81) and applying Jensen's inequality leads to

$$\sum_{i \in \mathcal{I}} r_{k_j+1-i}^2 \geq \frac{1}{|\mathcal{I}|p^2c^2}, \quad \forall j \in \mathbb{N}. \quad (82)$$

By summing property (61) with  $\Psi$  introduced in (38),  $k = k_j + 1 - i$  and for  $i \in \mathcal{I}$ , and using (82), we get the following inequality

$$\frac{a}{|\mathcal{I}|p^2c^2} \leq \sum_{i \in \mathcal{I}} (\Psi(x_{k_j+1-i}, \dots, x_{k_j+1-i-N}) - \Psi(x_{k_j+2-i}, \dots, x_{k_j+2-i-N})), \quad \forall j \in \mathbb{N}. \quad (83)$$

On the other hand, since  $\lim_{k \rightarrow \infty} x_k = x^*$  and  $\Psi$  is a continuous function, we have that

$$\lim_{j \rightarrow \infty} (\Psi(x_{k_j+1-i}, \dots, x_{k_j+1-i-N}) - \Psi(x_{k_j+2-i}, \dots, x_{k_j+2-i-N})) = 0,$$

which contradicts (83). Then item (i) follows.

We now consider items (ii) and (iii). From Corollary 4.1, there exists a unique point  $x^* \in \mathbb{R}^n$  such that  $\lim_{k \rightarrow \infty} x_k = x^*$ . Let  $U$  and  $\nu$  be such that Definition 2.4 is satisfied for the function  $\Psi$  at the point  $(x^*, \dots, x^*)$ . Thanks to Lemma 4.3 and Corollary 4.1, we have  $(x_k, x_{k-1}, \dots, x_{k-N}) \in U \cap \{y \in \mathbb{R}^n \times \dots \times \mathbb{R}^n : \Psi(x^*, \dots, x^*) < \Psi(y) < \Psi(x^*, \dots, x^*) + \nu\}$  for all sufficiently large  $k \in \mathbb{N}$ ; with abuse of notation, we will assume such an inclusion holds for all  $k \in \mathbb{N}$ . Then, the KL inequality can be evaluated at the point  $(x_k, x_{k-1}, \dots, x_{k-N})$ , i.e.,

$$\xi'(\Psi(x_k, x_{k-1}, \dots, x_{k-N}) - \Psi(x^*, x^*, \dots, x^*)) \|\nabla \Psi(x_k, x_{k-1}, \dots, x_{k-N})\| \geq 1.$$

By recalling that  $\xi(t) = ct^{1-\theta}$ , and squaring both sides of the above inequality, we obtain

$$(\Psi(x_k, x_{k-1}, \dots, x_{k-N}) - \Psi(x^*, x^*, \dots, x^*))^{2\theta} \leq c^2 \|\nabla \Psi(x_k, x_{k-1}, \dots, x_{k-N})\|^2. \quad (84)$$

Note that

$$\nabla \Psi(z_1, z_2, \dots, z_{N+1}) = \begin{pmatrix} \nabla F(z_1) + \gamma(z_1 - z_2) \\ \gamma(z_2 - z_1 + z_2 - z_3) \\ \vdots \\ \gamma(z_N - z_{N-1} + z_N - z_{N+1}) \\ \gamma(z_{N+1} - z_N) \end{pmatrix}.$$

Therefore, from inequality (84) we get

$$\begin{aligned} (\Psi(x_k, x_{k-1}, \dots, x_{k-N}) - \Psi(x^*, x^*, \dots, x^*))^{2\theta} &\leq c^2 \left( \|\nabla F(x_k)\| + 2\gamma \sum_{j=1}^N \|x_{k+1-j} - x_{k-j}\| \right)^2 \\ &\leq 2c^2 \|\nabla F(x_k)\|^2 + 8c^2 \gamma^2 N \sum_{j=1}^N \|x_{k+1-j} - x_{k-j}\|^2 \\ &\leq 2c^2 \|\nabla F(x_k)\|^2 + 16c^2 \alpha_{\max} \mu \left( \sqrt{1 + \frac{\tau}{2}} + \sqrt{\frac{\tau}{2}} \right)^2 \gamma^2 N \sum_{j=1}^N (-h_{k-j}(\tilde{y}_{k-j})), \end{aligned}$$

where the second inequality follows by applying relation  $(u + v)^2 \leq 2u^2 + 2v^2$  and Jensen's inequality, and the third inequality holds by combining (55) and (36). We continue by applying (59) and Lemma 4.4 to the above inequality, thus obtaining

$$\begin{aligned} (\Psi(x_k, x_{k-1}, \dots, x_{k-N}) - \Psi(x^*, x^*, \dots, x^*))^{2\theta} &\leq 4b^2 c^2 \sum_{j=-(N-1)}^N (-h_{k+j-1}(\tilde{y}_{k+j-1})) \\ &+ 8N^2 L_f^2 \alpha_{\max} \mu c^2 \left( 1 + \frac{\tau}{2} \right) (-h_k(\tilde{y}_k)) + 16c^2 \alpha_{\max} \mu \left( \sqrt{1 + \frac{\tau}{2}} + \sqrt{\frac{\tau}{2}} \right)^2 \gamma^2 N \sum_{j=1}^N (-h_{k-j}(\tilde{y}_{k-j})). \end{aligned}$$

In conclusion, there exists a sufficiently large  $\tilde{b} > 0$  such that

$$(\Psi(x_k, x_{k-1}, \dots, x_{k-N}) - \Psi(x^*, x^*, \dots, x^*))^{2\theta} \leq \tilde{b} \sum_{j=-(N-1)}^N (-h_{k+j-1}(\tilde{y}_{k+j-1})),$$

and an application of Lemma 4.3 implies

$$\begin{aligned} & (\Psi(x_k, x_{k-1}, \dots, x_{k-N}) - \Psi(x^*, x^*, \dots, x^*))^{2\theta} \\ & \leq \frac{\tilde{b}}{\sigma \lambda_{\min}} \sum_{j=-(N-1)}^N (\Psi(x_{k+j-1}, x_{k+j-2}, \dots, x_{k+j-1-N}) - \Psi(x_{k+j}, x_{k+j-1}, \dots, x_{k+j-N})) \\ & = \frac{\tilde{b}}{\sigma \lambda_{\min}} (\Psi(x_{k-N}, x_{k-N-1}, \dots, x_{k-2N}) - \Psi(x_{k+N}, x_{k+N-1}, \dots, x_k)). \end{aligned}$$

Setting  $k = \tilde{k}N$  with  $\tilde{k} \in \mathbb{N}$  yields

$$\begin{aligned} & (\Psi(x_{\tilde{k}N}, x_{\tilde{k}N-1}, \dots, x_{(\tilde{k}-1)N}) - \Psi(x^*, x^*, \dots, x^*))^{2\theta} \\ & \leq \frac{\tilde{b}}{\sigma \lambda_{\min}} (\Psi(x_{(\tilde{k}-1)N}, x_{(\tilde{k}-1)N-1}, \dots, x_{(\tilde{k}-2)N}) - \Psi(x_{(\tilde{k}+1)N}, x_{(\tilde{k}+1)N-1}, \dots, x_{\tilde{k}N})). \end{aligned} \quad (85)$$

By defining the following sequence

$$\Delta_{\tilde{k}} = \Psi(x_{\tilde{k}N}, x_{\tilde{k}N-1}, \dots, x_{(\tilde{k}-1)N}) - \Psi(x^*, x^*, \dots, x^*), \quad \forall \tilde{k} \in \mathbb{N}, \quad (86)$$

we can rewrite inequality (85) as follows

$$\Delta_{\tilde{k}}^{2\theta} \leq \frac{\tilde{b}}{\sigma \lambda_{\min}} (\Delta_{\tilde{k}-1} - \Delta_{\tilde{k}+1}), \quad \forall \tilde{k} \in \mathbb{N}. \quad (87)$$

Since  $\{\Delta_{\tilde{k}}\}_{\tilde{k} \in \mathbb{N}}$  is monotone non increasing by Lemma 4.3, we have  $\Delta_{\tilde{k}+1}^{2\theta} \leq \Delta_{\tilde{k}}^{2\theta}$ . Hence, by setting  $\tilde{c} = \tilde{b}/(\sigma \lambda_{\min})$ , inequality (87) yields

$$\Delta_{\tilde{k}+1}^{2\theta} \leq \tilde{c}(\Delta_{\tilde{k}-1} - \Delta_{\tilde{k}+1}), \quad \forall \tilde{k} \in \mathbb{N}.$$

At this point, items (ii) and (iii) follow by applying Lemma 4.7 and observing that

$$\Delta_{\tilde{k}} = \Psi(x_{\tilde{k}N}, x_{\tilde{k}N-1}, \dots, x_{(\tilde{k}-1)N}) - F(x^*) \geq F(x_{\tilde{k}N}) - F(x^*).$$

□

## 5 Numerical experiments

This section aims to assess the effectiveness of Block-PHILA in solving image deblurring and super-resolution problems, formulated within the Plug-and-Play framework. Specifically, assuming additive Gaussian noise with standard deviation  $\sigma \in \mathbb{R}^+$ , we consider the following PnP optimization problem

$$\operatorname{argmin}_{x \in \mathbb{R}^n} F(x) \equiv \frac{1}{2} \|Ax - b\|^2 + \frac{\lambda}{2} \|x - N_\sigma(x)\|^2, \quad (88)$$

which can be minimized by Block-PHILA adopting the following splitting of the objective function:

$$\begin{cases} \phi(x) = \frac{1}{2} \|Ax - b\|^2 \\ f(x) = \frac{\lambda}{2} \|x - N_\sigma(x)\|^2 \end{cases}. \quad (89)$$

An appropriate choice of the degradation matrix  $A$  allows us to address either deblurring or super-resolution tasks. The function  $N_\sigma$  is the UNet proposed in [49] and subsequently trained within the context of GS denoiser in [29]. We remark that the authors of [29] replaced the ReLU activation functions in the original UNet in [49] with eLU functions, in order to ensure the differentiability of  $N_\sigma$  with respect to its input. Hence, in our tests, we use the network’s weights released with the code of [29] within the DeepInverse library [42]. For the restricted denoiser we selected the patches of the image extending them with a padding contour having size 16 pixels.

The following different versions of Block-PHILA are implemented and compared.

**Block-PHILA-v1** corresponds to Algorithm 1 equipped with an adaptive Barzilai-Borwein rule for the steplength selection and a FISTA-like strategy for defining the sequence  $\{\beta_k\}_{k \in \mathbb{N}}$ . More precisely, the steplength  $\alpha_k$  is determined as the geometric mean of the two well-known Barzilai-Borwein rules, as proposed in [3]:

$$\alpha_k = \max \left\{ \alpha_{\min}, \min \left\{ \alpha_{\max}, \frac{\|U_{i_k}^T(x_k - x_{k-N})\|}{\|U_{i_k}^T(\nabla f(x_k) - \nabla f(x_{k-N}))\|} \right\} \right\}. \quad (90)$$

On the other hand, by following the strategy in [17], we set

$$\beta_k = \frac{\text{div}(k, N) - 1}{\text{div}(k, N) + 2}, \quad (91)$$

where  $\text{div}(\cdot, \cdot)$  denotes the integer division. Although rule (91) is usually chosen for Nesterov-like accelerated methods, it has also been employed for Heavy-Ball-like inertial terms, see e.g. [36]. The other parameters related to the inertial term are set as  $\beta_{\max} = 1$  and  $\gamma = 10^{-4}$ .

**Block-PHILA-v2** corresponds to Algorithm 1 where  $\alpha_k$  is fixed as in (90) and the inertial term is discarded, i.e.,  $\beta_k = 0$  and  $\gamma = 0$ .

**Block-PHILA-v3** corresponds to Algorithm 1 where the steplength is kept constant throughout the iterations, namely  $\alpha_k = 1/\lambda$ , while  $\beta_k$  is defined as in (91),  $\gamma = 10^{-4}$  and  $\beta_{\max} = 1$ .

**Block-PHILA-v4** corresponds to Algorithm 1 where  $\alpha_k = 1/\lambda$ ,  $\beta_k = 0$  and  $\gamma = 0$ .

The remaining parameters are fixed across all versions as follows:  $\alpha_{\min} = 10^{-2}$ ,  $\alpha_{\max} = 10^3$ ,  $\delta = 0.5$ ,  $\sigma = 10^{-4}$  and  $\tau = 10^6$ . In addition, the scaling matrix is always chosen as the identity. The comparison among several parameter settings allows to highlight more clearly the contributions of the different components (steplengths, scaling matrices and inertial terms) defining Block-PHILA.

We remark that, for  $N = 1$ , Block-PHILA-v1 and Block-PHILA-v3 reduce to the PHILA approach proposed in [13] equipped with two particular hyperparameter settings. Similarly, Block-PHILA-v2 and Block-PHILA-v4 are special instances of the VMILA method developed in [10].

Since the optimization problem (88) is continuously differentiable, it can also be cast into the formulation (1) with

$$\begin{cases} f(x) = \frac{1}{2}\|Ax - b\|^2 + \frac{\lambda}{2}\|x - N_\sigma(x)\|^2 \\ \phi(x) = 0 \end{cases}. \quad (92)$$

As a consequence, we consider variants of Algorithm 1, named **Block-PHILA (v5–v8)**, where  $f$  and  $\phi$  are defined as in (92) and the settings of the other parameters are analogous to those of Block-PHILA (v1–v4), respectively.

The following sections present numerical results for Block-PHILA (v1–v8) by varying the number  $N$  of blocks. In the case of  $N = 1$ , we compare Block-PHILA with the GS-PnP algorithm [29], a state-of-the-art Plug-and-Play approach that has recently gained popularity for solving image restoration problems of the form (88). More specifically, GS-PnP is based on the forward-backward iteration (4) applied to the splitting (89). For GS-PnP, we used the authors’ official implementation<sup>1</sup> with the default hyperparameters setting.

<sup>1</sup><https://github.com/samuro95/GSPnP>

## 5.1 Image deblurring

In this section, we report results for problem (88), where  $A = H$  is defined as a convolution operator with circular boundary conditions. In particular, the operator  $H$  corresponds to a Gaussian blur kernel of size  $25 \times 25$  with standard deviation 1.6 [29, 39]. As reference images, we consider those from the Set3C dataset (*Butterfly*, *Starfish*, and *Leaves*). Furthermore, the observed data  $b$  are assumed to be corrupted by Gaussian noise with noise level  $\nu = 0.03$ . By following [29], where the authors consider the same test problems, we fixed  $\sigma = 1.8\nu$  and  $\lambda = 0.075$  in (88). All the compared algorithms were initialized using  $x_0 = b$ . Both Block-PHILA (v1–v4) and GS-PnP require the computation of the proximal operator of the data fidelity term in the backward step. For  $N = 1$ , a well-known closed-form solution can be applied, while for  $N > 1$ , an inexact procedure is used in the implementation of STEP 3 of Block-PHILA. Further details are provided in Appendix B and Appendix C, respectively.

Table 1 presents the results achieved by Block-PHILA (v1–v8) across different numbers of blocks; for  $N = 1$ , a comparison with GS-PnP is also provided. Specifically, given the stopping criterion

$$\frac{|F(x_{k+1}) - F(x_k)|}{|F(x_k)|} \leq \varepsilon, \quad (93)$$

with  $\varepsilon = 10^{-5}$ , Table 1 reports the values of the objective function and PSNR obtained by the different methods once (93) is satisfied, together with the corresponding number of iterations and computational time. For each combination of image and number of blocks, the best PSNR values are highlighted in bold, and the lowest computational times are underlined. The following considerations can be deduced from the analysis of Table 1.

- (i) For  $N = 1$  and for all tested images, Block-PHILA (v1–v3) meets the stopping criterion earlier than the competitors, while still providing comparable or better values for both the objective function and PSNR. These results highlight the advantages, in terms of convergence speed, of adopting an adaptive steplength  $\alpha_k$  and/or incorporating an inertial term, features absent in Block-PHILA-v4 and GS-PnP. The acceleration of standard forward-backward algorithms through adaptive steplengths and inertial techniques is well established in the literature, with their effectiveness having been repeatedly observed in imaging tasks (see, for example, [10, 13, 14, 19] and references therein), and our findings provide further confirmation of these benefits. Moreover, for  $N = 1$ , versions v1–v4 of Block-PHILA, based on the splitting (89) of the objective function, typically outperform Block-PHILA (v5–v8), which instead exploit the differentiability of both the fidelity and regularization terms by adopting the splitting (92). This behaviour has already been observed in [20].
- (ii) For  $N = 2$  and  $N = 4$ , Block-PHILA (v1–v4) consistently outperforms Block-PHILA (v5–v8) in terms of PSNR achieved when the stopping criterion is satisfied. Although Block-PHILA-v8 sometimes satisfies the stopping criterion earlier than its forward-backward counterpart Block-PHILA-v4, this is not due to faster convergence; rather, it results from stalled progress in the objective function values between successive iterations. Indeed, the PSNR values provided by Block-PHILA-v8 are consistently the lowest.
- (iii) The performance of Block-PHILA for  $N > 1$  is comparable to that obtained for  $N = 1$  in terms of objective function reduction and PSNR values. Notably, the block-wise structure facilitates the processing of large-scale images more efficiently, enabling scalable optimization without compromising performance. This design also significantly reduces GPU memory usage, making the method well-suited for high-resolution data and resource-constrained environments.

Similar conclusions can be drawn from Figure 2, which reports the PSNR and objective function values achieved by some of the compared methods on the *Leaves* image with respect to the computational time. In particular, panels (a)–(c) and (d)–(f) report the PSNR and objective function values obtained by Block-PHILA-v1 and Block-PHILA-v7, respectively, for different numbers of blocks. For  $N = 1$ ,

		<i>Butterfly</i>				<i>Leaves</i>				<i>Starfish</i>			
		<i>F</i>	PSNR	itr	time	<i>F</i>	PSNR	itr	time	<i>F</i>	PSNR	itr	time
$N = 1$	GS-PnP	97.50	28.17	30	4.48	97.72	28.41	42	6.10	97.73	28.99	23	3.30
	Block-PHILA-v1	97.65	27.55	7	<u>1.30</u>	97.72	<b>28.55</b>	21	3.29	97.81	28.72	7	<u>1.29</u>
	Block-PHILA-v2	97.50	28.23	15	2.69	97.73	28.40	15	<u>2.61</u>	97.74	28.97	15	2.68
	Block-PHILA-v3	97.50	<b>28.42</b>	13	2.12	97.73	28.49	18	2.76	97.73	<b>29.13</b>	15	2.45
	Block-PHILA-v4	97.50	28.17	30	4.76	97.72	28.41	42	6.77	97.73	28.99	23	3.65
	Block-PHILA-v5	97.58	27.49	37	9.80	98.19	26.61	31	8.58	97.79	28.66	37	10.64
	Block-PHILA-v6	97.62	27.23	56	14.56	98.20	26.56	40	10.44	97.78	28.68	55	15.22
	Block-PHILA-v7	97.71	26.89	28	6.63	97.86	27.66	60	14.20	97.78	28.76	40	9.39
	Block-PHILA-v8	97.69	26.93	43	10.48	98.27	26.37	37	8.91	98.40	27.58	8	1.75
$N = 2$	Block-PHILA-v1	97.54	28.12	21	3.37	97.77	28.47	24	<u>3.73</u>	97.85	28.75	13	2.10
	Block-PHILA-v2	97.56	27.64	23	4.30	97.89	27.67	23	3.80	97.79	28.72	21	3.88
	Block-PHILA-v3	97.53	<b>28.23</b>	20	<u>2.87</u>	97.74	<b>28.49</b>	37	5.59	97.80	28.84	13	<u>2.02</u>
	Block-PHILA-v4	97.52	28.02	46	6.72	97.74	28.35	70	10.64	97.75	<b>28.88</b>	32	5.00
	Block-PHILA-v5	97.70	26.88	53	13.28	98.12	26.78	67	17.73	97.81	28.50	57	15.48
	Block-PHILA-v6	97.95	26.22	43	10.72	98.48	25.94	44	11.32	97.95	28.05	36	9.33
	Block-PHILA-v7	97.84	26.48	41	9.59	98.16	26.67	61	14.63	97.78	28.62	68	16.84
	Block-PHILA-v8	98.71	25.43	15	3.29	98.67	25.63	42	10.16	97.90	28.19	46	11.60
$N = 4$	Block-PHILA-v1	97.63	27.43	29	<u>4.28</u>	97.79	<b>28.43</b>	45	<u>7.24</u>	97.79	<b>28.99</b>	36	6.00
	Block-PHILA-v2	97.58	27.53	41	6.63	97.93	27.52	43	7.31	98.00	28.37	24	4.39
	Block-PHILA-v3	97.54	<b>28.13</b>	37	4.95	97.78	28.39	52	7.54	97.81	28.79	25	<u>3.72</u>
	Block-PHILA-v4	97.55	27.77	67	9.23	97.80	28.07	92	13.47	97.77	28.85	59	8.90
	Block-PHILA-v5	97.84	26.48	80	19.67	99.05	25.29	49	12.56	97.93	28.12	59	15.22
	Block-PHILA-v6	97.90	26.33	90	22.68	98.26	26.37	140	37.56	98.00	27.95	59	15.43
	Block-PHILA-v7	98.56	25.60	29	6.20	98.28	26.33	98	23.73	97.96	28.02	52	12.56
	Block-PHILA-v8	98.78	25.40	31	6.78	98.57	25.77	94	22.82	98.22	27.72	36	8.75

Table 1: Results achieved by Block-PHILA (v1-v8) in solving the image deblurring problems by varying the number  $N$  of blocks. For  $N = 1$  the results obtained by GS-PnP are also included. For each image and value of  $N$ , the best PSNR is shown in bold and the lowest time is underlined.

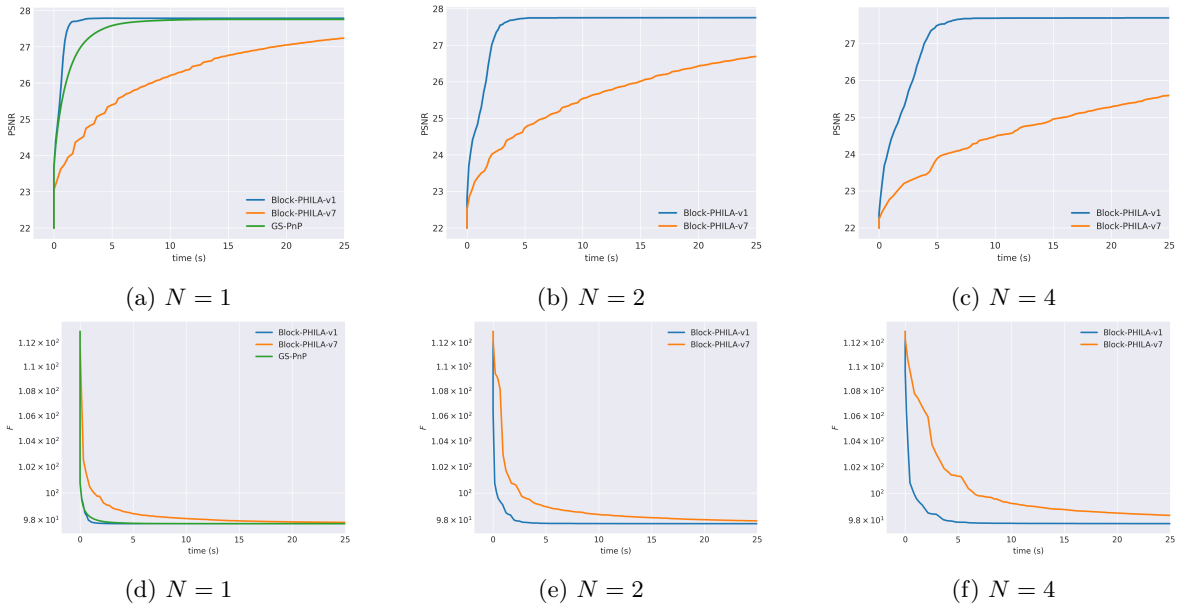


Figure 2: Results achieved solving the image deblurring problem on *leaves* by varying the number  $N$  of blocks. For  $N = 1$  the results obtained by GS-PnP are also included.

the results obtained by GS-PnP are also included. It is evident that Block-PHILA-v1 consistently outperforms both Block-PHILA-v7 and GS-PnP for  $N = 1$ . Moreover, its performance does not degrade as the number of blocks increases.

Finally, in Figure 3 we compare the reconstructions obtained by GS-PnP, Block-PHILA-v1, and Block-PHILA-v7 (for different numbers of blocks) after 2 seconds of computation. Following [29], a further application of the denoiser  $D_\sigma$ , defined in (2), is also performed on the last iterate. For  $N = 1$  Block-PHILA-v1 yields the best approximation of the solution, achieving high overall sharpness and well-preserved edges. For  $N = 2$  and  $N = 4$ , Block-PHILA-v1 also provides satisfactory reconstructions, effectively removing noise and blur without introducing block artifacts. In contrast, Block-PHILA-v7 exhibits the worst reconstruction behavior. This is particularly evident for  $N = 1$ , where the solution obtained with Block-PHILA-v1 is of significantly higher quality.

## 5.2 Image super-resolution

In this section, we consider problem (88) with  $A = SH$ , where  $H \in \mathbb{R}^{n \times n}$  is a convolution operator with anti-aliasing kernel and  $S \in \mathbb{R}^{m \times n}$  is a standard  $s$ -fold downsampling matrix such that  $n = s^2 \times m$ . Specifically, the blur operator  $H$  is the same as that used in the image deblurring problems discussed in Section 5.1, while the downsampled images correspond to a scale factor  $s = 2$ . The data  $b \in \mathbb{R}^n$  represents a low-resolution image obtained by the high-resolution image  $x \in \mathbb{R}^n$  via  $y = SHx + \eta$ , where both the reference images and the noise  $\eta$  are set as in Section 5.1. The values for  $\sigma$  and  $\lambda$  in (88) are fixed to  $2\nu$  and 0.065, respectively, following [29], where the same test problem was considered. All the compared algorithms were initialized using as  $x_0$  a bicubic interpolation of  $b$  (with a proper shift correction as suggested in [49]). We refer again the reader to Appendix B and Appendix C for the computation of the proximal point needed by Block-PHILA (v1-v4) and GS-PnP.

Table 2 reports the objective function values, PSNR, number of iterations, and computational times achieved by the compared methods when condition (93) is satisfied with  $\varepsilon = 10^{-5}$ . For each image and block configuration, the highest PSNR values are in bold, while the lowest computational times are underlined. Figure 4 reports the PSNR and objective function values achieved by Block-

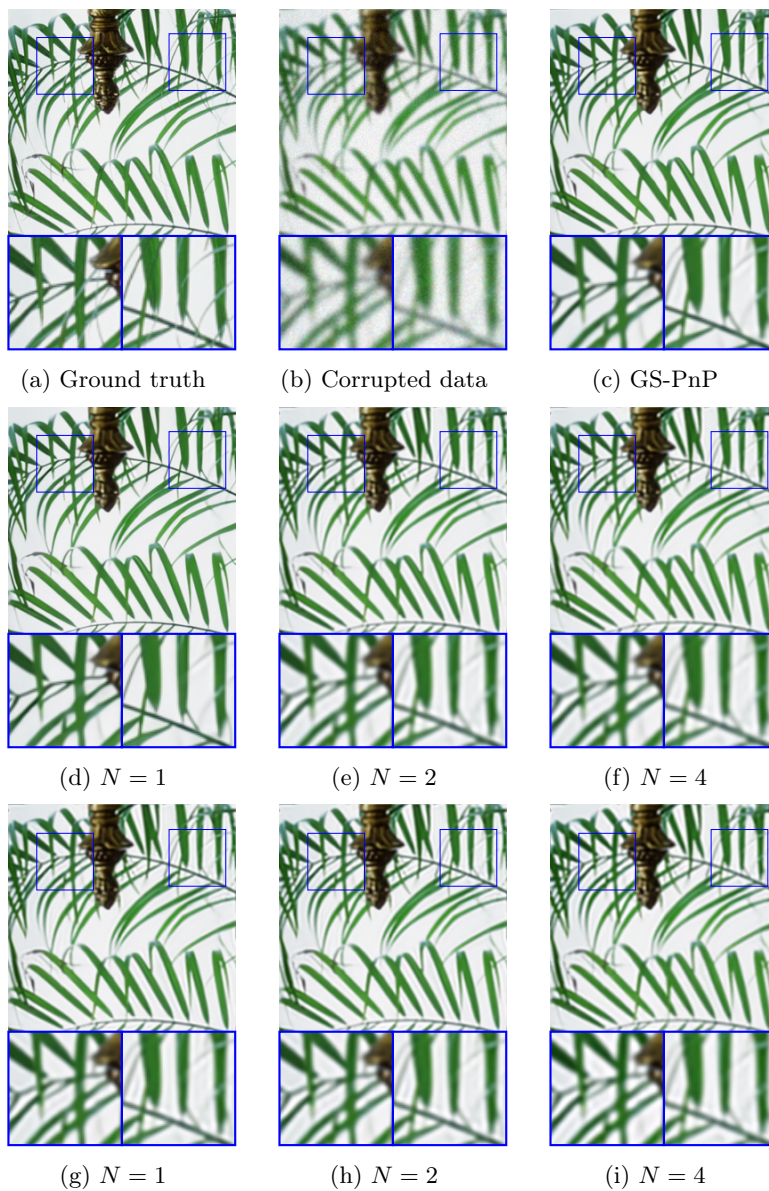


Figure 3: Reconstructions provided by GS-PnP, Block-PHILA-v1 (second row) and Block-PHILA-v7 (third row) for the image deblurring problem.

		<i>Butterfly</i>				<i>Leaves</i>				<i>Starfish</i>			
		<i>F</i>	PSNR	itr	time	<i>F</i>	PSNR	itr	time	<i>F</i>	PSNR	itr	time
$N = 1$	GS-PnP	33.86	26.78	45	8.59	34.04	26.79	66	14.07	34.30	27.43	30	6.35
	Block-PHILA-v1	33.86	26.93	21	3.58	34.03	<b>26.92</b>	24	<u>4.26</u>	34.30	<b>27.47</b>	18	3.22
	Block-PHILA-v2	33.91	26.52	13	<u>2.22</u>	34.04	26.80	28	5.51	34.31	27.43	16	<u>2.95</u>
	Block-PHILA-v3	33.86	<b>26.99</b>	24	4.23	34.03	26.91	33	6.13	34.31	27.46	21	3.79
	Block-PHILA-v4	33.86	26.78	45	8.23	34.04	26.79	66	12.47	34.30	27.43	30	5.58
	Block-PHILA-v5	33.89	26.53	33	10.03	34.05	26.73	70	22.98	34.31	27.43	37	12.18
	Block-PHILA-v6	33.88	26.60	52	16.39	34.09	26.42	62	21.26	34.32	27.38	43	13.95
	Block-PHILA-v7	33.86	26.86	28	5.86	34.04	26.80	34	7.38	34.30	<b>27.47</b>	26	5.53
	Block-PHILA-v8	33.92	26.29	39	8.90	34.13	26.18	49	11.93	34.31	27.41	49	11.96
$N = 2$	Block-PHILA-v1	33.88	<b>27.07</b>	25	<u>4.13</u>	34.08	26.80	22	<u>3.49</u>	34.31	27.46	30	5.07
	Block-PHILA-v2	33.92	26.25	24	4.56	34.11	26.32	35	6.75	34.33	27.35	23	<u>4.42</u>
	Block-PHILA-v3	33.87	27.03	34	5.51	34.04	<b>26.90</b>	61	10.46	34.31	<b>27.47</b>	34	6.43
	Block-PHILA-v4	33.87	26.71	74	12.54	34.05	26.71	104	18.98	34.31	27.41	52	9.46
	Block-PHILA-v5	33.95	26.07	45	12.30	34.08	26.43	90	26.81	34.36	27.17	34	9.46
	Block-PHILA-v6	33.91	26.26	72	20.96	34.26	25.56	54	16.65	34.35	27.25	48	13.67
	Block-PHILA-v7	33.88	26.72	40	7.54	34.07	26.62	45	8.53	34.31	27.46	37	7.52
	Block-PHILA-v8	33.91	26.29	77	14.56	35.19	25.48	59	12.30	34.32	27.34	73	16.92
$N = 4$	Block-PHILA-v1	33.91	<b>27.08</b>	40	<u>5.61</u>	34.09	26.79	44	<u>6.57</u>	34.33	<b>27.50</b>	42	<u>6.47</u>
	Block-PHILA-v2	33.94	26.19	42	6.52	34.23	25.76	42	6.69	34.35	27.28	42	6.48
	Block-PHILA-v3	33.88	27.00	63	9.32	34.06	<b>26.81</b>	73	12.12	34.33	<b>27.50</b>	48	7.55
	Block-PHILA-v4	33.89	26.50	107	16.73	34.08	26.53	152	27.01	34.33	27.32	72	12.49
	Block-PHILA-v5	34.12	25.33	44	10.80	34.16	25.97	115	34.37	34.36	27.20	69	19.42
	Block-PHILA-v6	33.92	26.15	119	32.85	34.29	25.42	105	29.98	34.38	27.07	76	22.52
	Block-PHILA-v7	33.96	26.11	47	7.90	34.12	26.26	68	12.57	34.31	27.45	68	12.43
	Block-PHILA-v8	33.99	25.85	100	17.86	34.60	25.60	126	23.94	34.82	27.27	128	26.00

Table 2: Results achieved by Block-PHILA (v1–v8) in solving the super-resolution problems by varying the number  $N$  of blocks. For  $N = 1$ , the results obtained by GS-PnP are also included. For each image and value of  $N$ , the best PSNR is shown in bold and the lowest time is underlined.

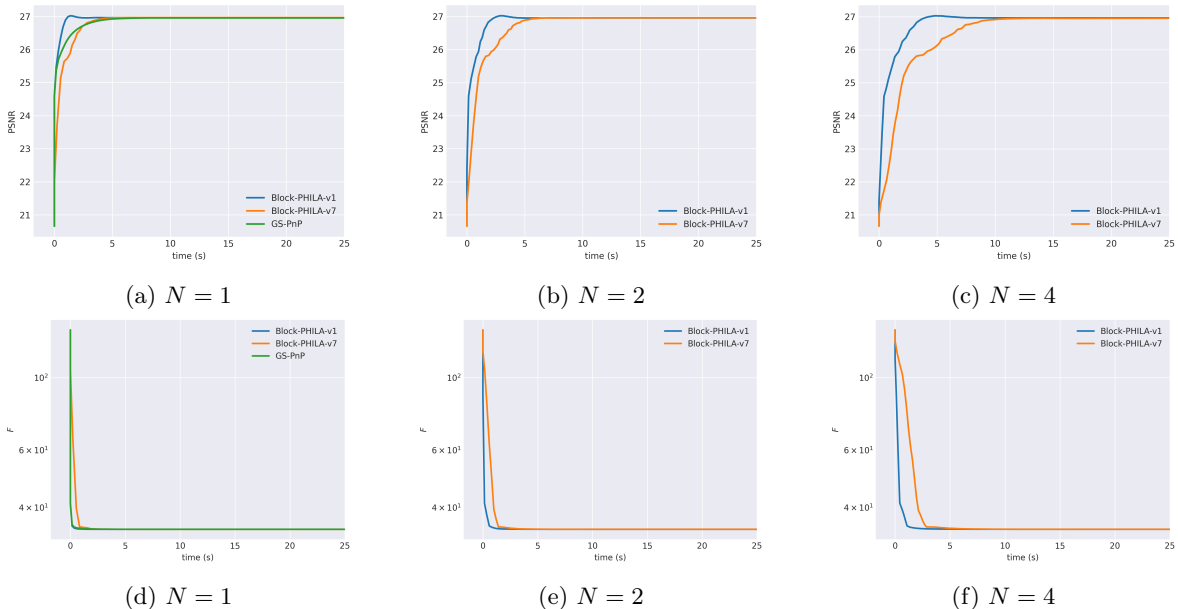


Figure 4: Results achieved solving the image super resolution problem on *starfish* by varying the number  $N$  of blocks. For  $N = 1$  the results obtained by GS-PnP are also included.

PHILA-v1 and Block-PHILA-v7 on the *Butterfly* image with respect to the computational time, for different numbers of blocks. In the case  $N = 1$ , the results obtained by GS-PnP are also included.

The results in Table 2 and Figure 4 are consistent with the conclusions drawn in Section 5.1 from the image deblurring experiments. In particular, across all tested images and block configurations, the Block-PHILA variants v1-v3 consistently satisfy the stopping criterion faster than the competing methods, while providing comparable or higher PSNR values. Moreover, the Block-PHILA versions v1-v4 based on the splitting (89) generally outperform those exploiting the differentiability of both the fidelity and regularization terms (v5-v8). This is further confirmed by Figure 5 which reports the reconstructions achieved by GS-PnP, Block-PHILA-v1 and Block-PHILA-v7 after a time budget of 2 seconds and an additional denoising step. For any number of blocks, Block-PHILA-v1 produces sharp and accurate reconstructions without the artifacts observed in Block-PHILA-v7 for  $N = 2$  or  $N = 4$ . We can conclude that the block-wise formulation remains advantageous for super-resolution, enabling efficient processing of possibly large-scale images with reduced memory usage and computational effort, while maintaining high reconstruction accuracy.

## 6 Conclusions

In this paper we introduced a general block-coordinate forward-backward framework for the solution of non-convex and non-separable optimization problems. Convergence of the sequence of the iterates and related rates have been proved within the Kurdyka-Łojasiewicz framework. Building upon this theoretical framework, we developed a novel block-coordinate PnP approach based on Gradient Step denoisers. By decomposing the image into contiguous patches and exploiting the structural properties of convolutional neural networks, the suggested approach enables an efficient block-wise computation of the term related to the Gradient Step denoiser. Numerical experiments on imaging tasks, such as deblurring and super-resolution, show that the proposed block-coordinate PnP algorithm attains state-of-the-art reconstruction performance while significantly lowering GPU memory usage. Future work may concern the extension of our proposed block-coordinate forward-backward framework to non-

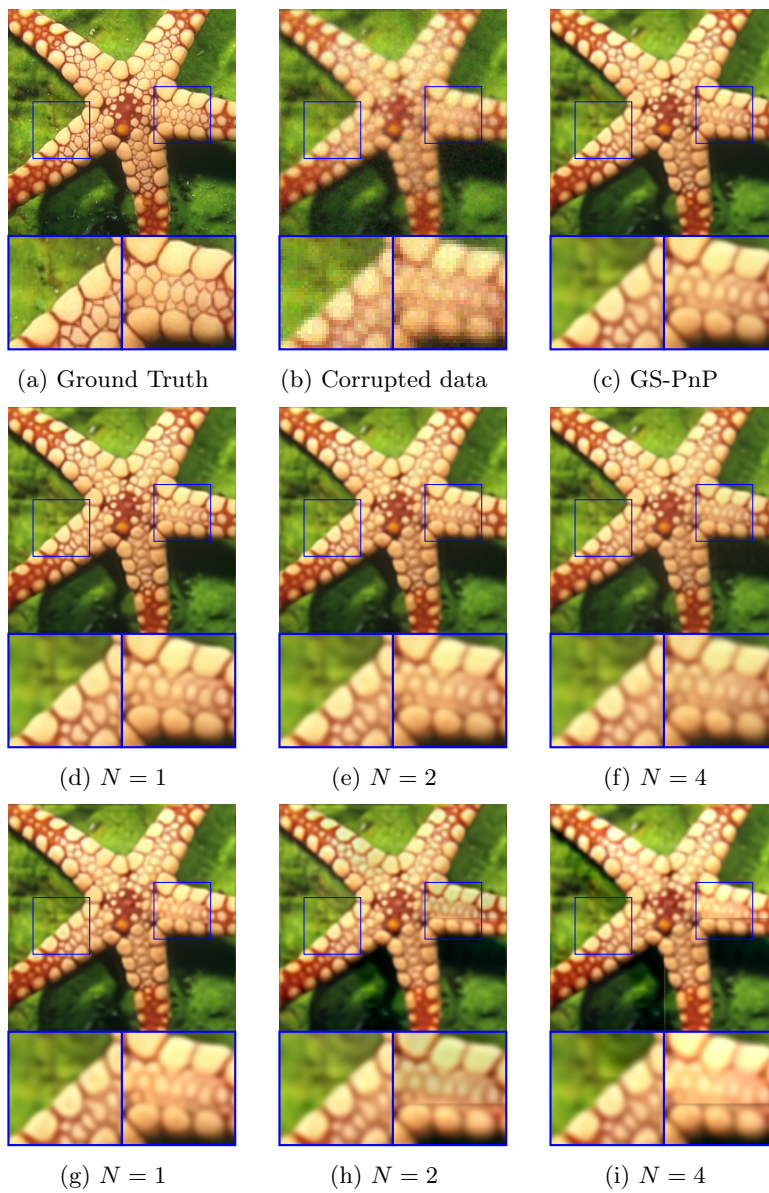


Figure 5: Reconstructions provided by GS-PnP, Block-PHILA-v1 (second row) and Block-PHILA-v7 (third row) for the super-resolution problem.

smooth objective functions, as well as the study of novel PnP line-search based approaches where the Gradient-Step denoiser replaces the proximal operator, rather than the gradient step, in the iterative procedure.

## Acknowledgments

All authors are members of the Gruppo Nazionale per il Calcolo Scientifico (GNCS) of the Italian Istituto Nazionale di Alta Matematica (INdAM), which is kindly acknowledged.

All authors are partially supported by the the Italian MUR through the PRIN 2022 PNRR Project “Advanced optimization METHods for automated central veIn Sign detection in multiple sclerosis from magneTic resonAnce imaging (AMETISTA)”, project code: P2022J9SNP (CUP E53D23017980001), under the National Recovery and Resilience Plan (PNRR), Italy, Mission 04 Component 2 Investment 1.1 funded by the European Commission - NextGeneration EU programme.

## References

- [1] A. ABERDAM AND A. BECK, *An Accelerated Coordinate Gradient Descent Algorithm for Non-separable Composite Optimization*, J. Optim. Theory and Appl., 193 (2022), pp. 219–246.
- [2] R. AHMAD, C. A. BOUMAN, G. T. BUZZARD, S. CHAN, S. LIU, E. T. REEHORST, AND P. SCHNITER, *Plug-and-Play Methods for Magnetic Resonance Imaging: Using Denoisers for Image Recovery*, IEEE Signal Process. Mag., 37 (2020), pp. 105–116.
- [3] C. AN AND X. XU, *Regularized Barzilai-Borwein method*, Numer. Algor., (2025).
- [4] H. ATTOUCH AND J. BOLTE, *On the convergence of the proximal algorithm for nonsmooth functions involving analytic features*, Math. Program., 116 (2009), pp. 5–16.
- [5] H. ATTOUCH, J. BOLTE, AND B. F. SVAITER, *Convergence of descent methods for semi-algebraic and tame problems: proximal algorithms, forward-backward splitting, and regularized Gauss-Seidel methods*, Math. Program., 137 (2013), pp. 91–129.
- [6] A. BECK, *First-Order Methods in Optimization*, Society for Industrial and Applied Mathematics, 2017.
- [7] M. BERTERO, H. LANTÉRI, AND L. ZANNI, *Iterative image reconstruction: a point of view*, Edizioni della Normale, Pisa, 2008, pp. 37–63.
- [8] J. BOLTE, A. DANILIDIS, AND S. M., *Clarke subgradients of stratifiable functions*, SIAM J. Optim., 10 (2007), pp. 556–572.
- [9] J. BOLTE, S. SABACH, AND M. TEBoulLE, *Proximal alternating linearized minimization for nonconvex and nonsmooth problems*, Math. Program., 146 (2014), pp. 459–494.
- [10] S. BONETTINI, I. LORIS, F. PORTA, AND M. PRATO, *Variable metric inexact line-search based methods for nonsmooth optimization*, SIAM J. Optim., 26 (2016), pp. 891–921.
- [11] S. BONETTINI, P. OCHS, M. PRATO, AND S. REBEGOLDI, *An abstract convergence framework with application to inertial inexact forward-backward methods*, Comput. Optim. Appl., 84 (2023), pp. 319–362.
- [12] S. BONETTINI, M. PRATO, AND S. REBEGOLDI, *A block coordinate variable metric linesearch based proximal gradient method*, Comput. Optim. Appl., 71 (2018), pp. 5–52.

- [13] ———, *A new proximal heavy ball inexact line-search algorithm*, *Comput. Optim. Appl.*, 88 (2024), pp. 525–565.
- [14] S. BONETTINI, S. REBEGOLDI, AND V. RUGGIERO, *Inertial variable metric techniques for the inexact forwardbackward algorithm*, *SIAM J. Sci. Comput.*, 40 (2018), pp. A3180–A3210.
- [15] G. T. BUZZARD, S. H. CHAN, S. SREEHARI, AND C. A. BOUMAN, *Plug-and-Play Unplugged: Optimization-Free Reconstruction Using Consensus Equilibrium*, *SIAM J. Imaging Sci.*, 11 (2018), pp. 2001–2020.
- [16] C. CASTERA, J. BOLTE, C. FÉVOTTE, AND E. PAUWELS, *An Inertial Newton Algorithm for Deep Learning*, *J. Mach. Learn. Res.*, 22 (2021), pp. 1–31.
- [17] A. CHAMBOLLE AND C. DOSSAL, *On the convergence of the iterates of FISTA*, *J. Optim. Theory Appl.*, 166 (2015), pp. 968–982.
- [18] F. CHOROBURA AND I. NECOARA, *Random Coordinate Descent Methods for Nonseparable Composite Optimization*, *SIAM J. Optim.*, 33 (2023), pp. 2160–2190.
- [19] E. CHOUZENOUX, J. PESQUET, AND A. REPETTI, *A block coordinate variable metric forward-backward algorithm*, *J. Glob. Optim.*, 66 (2016), pp. 457–485.
- [20] P. L. COMBETTES AND L. E. GLAUDIN, *Proximal Activation of Smooth Functions in Splitting Algorithms for Convex Image Recovery*, *SIAM J. Imaging Sci.*, 12 (2019), pp. 1905–1935.
- [21] D. DAVIS, D. DRUSVYATSKIY, S. KAKADE, AND J. LEE, *Stochastic Subgradient Method Converges on Tame Functions*, *Found. Comput. Math.*, 20 (2020), pp. 119–154.
- [22] P. FRANKEL, G. GARRIGOS, AND J. PEYPOUQUET, *Splitting methods with variable metric for Kurdyka-Łojasiewicz functions and general convergence rates*, *J. Opt. Theory Appl.*, 165 (2015), pp. 874–900.
- [23] W. GAN, S. SHOUSHARI, Y. HU, J. LIU, H. AN, AND U. S. KAMILOV, *Block coordinate plug-and-play methods for blind inverse problems*, in *Proceedings of the 37th International Conference on Neural Information Processing Systems, NIPS '23*, Red Hook, NY, USA, 2023, Curran Associates Inc.
- [24] D. GRISHCHENKO, F. IUTZELER, AND J. MALICK, *Proximal gradient methods with adaptive subspace sampling*, *Math. Oper. Res.*, 46 (2021), pp. 1303–1323.
- [25] E. GUR, S. SABACH, AND S. SHTERN, *Nested alternating minimization with FISTA for non-convex and non-smooth optimization problems*, *J. Optim. Theory Appl.*, 199 (2023), pp. 1130–1157.
- [26] F. HANZELY, K. MISHCHENKO, AND P. RICHTÁRIK, *SEGA: Variance reduction via gradient sketching*, *Adv. Neural. Inf. Process. Syst.*, 31 (2018).
- [27] J. B. HIRIART-URRUTY AND C. LEMARÉCHAL, *Convex analysis and minimization algorithms. II*, Springer-Verlag, Berlin, 1993.
- [28] C. HUANG, Z. WU, Y. CHENG, T. ZENG, C.-B. SCHÖNLIEB, AND A. I. AVILES-RIVERO, *Deep Block Proximal Linearized Minimization Algorithm for Nonconvex Inverse Problems*, *SIAM J. Math. Data Sci.*, 7 (2025), pp. 1729–1754.
- [29] S. HURAUULT, A. LECLAIRE, AND N. PAPADAKIS, *Gradient step denoiser for convergent Plug-and-Play*, in *International Conference on Learning Representations (ICLR)*, 2022.

- [30] P. LATAFAT, A. THEMELIS, AND P. PATRINOS, *Block-coordinate and incremental aggregated proximal gradient methods for nonsmooth nonconvex problems*, Math. Program., 193 (2022), pp. 195–224.
- [31] W. LUO, Y. LI, R. URTASUN, AND R. ZEMEL, *Understanding the Effective Receptive Field in Deep Convolutional Neural Networks*, Adv. Neural Inf. Process. Syst., (2016), pp. 4905–4913.
- [32] T. MEINHARDT, M. MOLLER, C. HAZIRBAS, AND D. CREMERS, *Learning proximal operators: Using denoising networks for regularizing inverse imaging problems*, in Proc. IEEE Int. Conf. Comput. Vis., 2017, pp. 1781–1790.
- [33] I. NECOARA AND F. CHOROBURA, *Efficiency of stochastic coordinate proximal gradient methods on nonseparable composite optimization*, Math. Oper. Res., 50 (2025), pp. 993–1018.
- [34] P. OCHS, *Unifying abstract inexact convergence theorems and block coordinate variable metric iPiano*, SIAM J. Optim., 29 (2019), pp. 541–570.
- [35] J.-C. PESQUET, A. REPETTI, M. TERRIS, AND Y. WIAUX, *Learning Maximally Monotone Operators for Image Recovery*, SIAM J. Imaging Sci., 14 (2021), pp. 1206–1237.
- [36] T. POCK AND S. SABACH, *Inertial Proximal Alternating Linearized Minimization (iPALM) for Nonconvex and Nonsmooth Problems*, SIAM J. Imaging Sci., 9 (2016), pp. 1756–1787.
- [37] S. REBEGOLDI, *Analysis of a variable metric block coordinate method under proximal errors*, Ann. Univ. Ferrara., 70 (2024), pp. 23–61.
- [38] E. T. REEHORST AND P. SCHNITER, *Regularization by denoising: Clarifications and new interpretations*, IEEE Trans. Comput. Imaging, 5 (2018), pp. 52–67.
- [39] Y. ROMANO, M. ELAD, AND P. MILANFAR, *The little engine that could: Regularization by denoising (RED)*, SIAM J. Imaging Sci., 10 (2017), pp. 1804–1844.
- [40] E. RYU, J. LIU, S. WANG, X. CHEN, Z. WANG, AND W. YIN, *Plug-and-play methods provably converge with properly trained denoisers*, in International Conference on Machine Learning (PMLR), 2019, pp. 5546–5557.
- [41] Y. SUN, J. LIU, AND U. S. KAMILOV, *Block Coordinate Regularization by Denoising*, IEEE Trans. Comput. Imaging, 6 (2020), pp. 908–921.
- [42] J. TACHELLA, M. TERRIS, S. HURAUULT, A. WANG, L. DAVY, J. SCANVIC, V. SECHAUD, R. VO, T. MOREAU, T. DAVIES, ET AL., *Deepinverse: A python package for solving imaging inverse problems with deep learning*, Journal of Open Source Software, 10 (2025), p. 8923.
- [43] S. V. VENKATAKRISHNAN, C. A. BOUMAN, AND B. WOHLBERG, *Plug-and-play priors for model based reconstruction*, in IEEE Global Conference on Signal and Information Processing, 2013, pp. 945–948.
- [44] C. R. VOGEL, *Computational methods for inverse problems*, SIAM, Philadelphia, 2002.
- [45] X. XU, Y. SUN, J. LIU, B. WOHLBERG, AND U. S. KAMILOV, *Provable convergence of plug-and-play priors with mmse denoisers*, IEEE Signal Process. Lett., 27 (2020), pp. 1280–1284.
- [46] Y. XU AND W. YIN, *A block coordinate descent method for regularized multiconvex optimization with applications to nonnegative tensor factorization and completion*, SIAM J. Imaging Sci., 6 (2013), pp. 1758–1789.
- [47] ———, *A globally convergent algorithm for nonconvex optimization based on block coordinate update*, J. Sci. Comput., 72 (2017), pp. 700–1734.

- [48] X. YUAN, Y. LIU, J. SUO, AND Q. DAI, *Plug-and-play algorithms for large-scale snapshot compressive imaging*, in Proceedings of the IEEE/CVF Conference on Computer Vision and Pattern Recognition (CVPR), 2020.
- [49] K. ZHANG, Y. LI, W. ZUO, L. ZHANG, L. V. GOOL, AND R. TIMOFTE, *Plug-and-Play Image Restoration With Deep Denoiser Prior*, IEEE Trans. Pattern Anal. Mach. Intell., 44 (2021), pp. 6360–6376.
- [50] N. ZHAO, Q. WEI, A. BASARAB, N. DOBIGEON, D. KOUAMÉ, AND J.-Y. TOURNERET, *Fast Single Image Super-Resolution Using a New Analytical Solution for  $\ell_2 - \ell_2$  Problems*, IEEE Trans. Image Process., 25 (2016), pp. 3683–3697.

## A Proof of Lemma 4.7

The following proof is obtained by slightly modifying the arguments of [4, Theorem 2].

**Case  $\theta \in (\frac{1}{2}, 1)$ .** Let  $R \in (1, +\infty)$ . We distinguish between two cases.

- Assume first that  $\Delta_{k+1}^{-2\theta} \leq R\Delta_{k-1}^{-2\theta}$ . Then, from (77), we get the following chain of inequalities:

$$\begin{aligned}
1 &\leq \tilde{c}(\Delta_{k-1} - \Delta_{k+1})\Delta_{k+1}^{-2\theta} \\
&\leq R\tilde{c}(\Delta_{k-1} - \Delta_{k+1})\Delta_{k-1}^{-2\theta} \\
&\leq R\tilde{c} \int_{\Delta_{k+1}}^{\Delta_{k-1}} s^{-2\theta} ds \\
&= \frac{R\tilde{c}}{1-2\theta} (\Delta_{k-1}^{1-2\theta} - \Delta_{k+1}^{1-2\theta}),
\end{aligned}$$

where the third inequality follows from  $\Delta_{k-1}^{-2\theta} \leq s^{-2\theta}$  for all  $s \in [\Delta_{k+1}, \Delta_{k-1}]$  (the function  $s \rightarrow s^{-2\theta}$  is monotone decreasing) and the monotonicity of the integral. Setting

$$\mu = \frac{2\theta - 1}{R\tilde{c}} > 0, \quad \nu = 1 - 2\theta < 0,$$

one obtains

$$1 \leq -\frac{1}{\mu}(\Delta_{k-1}^\nu - \Delta_{k+1}^\nu) \Leftrightarrow 0 < \mu \leq \Delta_{k+1}^\nu - \Delta_{k-1}^\nu. \quad (94)$$

- Assume now that  $\Delta_{k+1}^{-2\theta} > R\Delta_{k-1}^{-2\theta}$ . Then

$$\begin{aligned}
\Delta_{k+1}^{-2\theta} > R\Delta_{k-1}^{-2\theta} &\Leftrightarrow \Delta_{k-1}^{2\theta} > R\Delta_{k+1}^{2\theta} \\
&\Leftrightarrow R^{-\frac{1}{2\theta}}\Delta_{k-1} > \Delta_{k+1} \\
&\Leftrightarrow R^{-\frac{1-2\theta}{2\theta}}\Delta_{k-1}^\nu < \Delta_{k+1}^\nu \\
&\Leftrightarrow (R^{\frac{2\theta-1}{2\theta}} - 1)\Delta_{k-1}^\nu < \Delta_{k+1}^\nu - \Delta_{k-1}^\nu,
\end{aligned}$$

where the direction of the third inequality changes due to  $\nu < 0$ . Since  $R^{\frac{2\theta-1}{2\theta}} - 1 > 0$  and  $\lim_{k \rightarrow \infty} \Delta_k = 0^+$ , there exists  $\tilde{\mu} > 0$  such that  $(R^{\frac{2\theta-1}{2\theta}} - 1)\Delta_{k-1}^\nu > \tilde{\mu}$  for all  $k \in \mathbb{N}$  for which  $\Delta_{k+1}^{-2\theta} > R\Delta_{k-1}^{-2\theta}$ . Therefore we obtain

$$0 < \tilde{\mu} \leq \Delta_{k+1}^\nu - \Delta_{k-1}^\nu. \quad (95)$$

By setting  $\hat{\mu} = \min\{\mu, \tilde{\mu}\}$  and combining (94) and (95), one gets

$$\Delta_{k+1}^\nu - \Delta_{k-1}^\nu \geq \hat{\mu} > 0, \quad \forall k \in \mathbb{N}.$$

By summing the above inequality for  $k = 1, \dots, K$ , we obtain

$$\begin{aligned} \sum_{k=1}^K (\Delta_{k+1}^\nu - \Delta_{k-1}^\nu) \geq \hat{\mu}K &\Leftrightarrow \sum_{k=1}^K (\Delta_{k+1}^\nu - \Delta_k^\nu) + \sum_{k=1}^K (\Delta_k^\nu - \Delta_{k-1}^\nu) \geq \hat{\mu}K \\ &\Leftrightarrow \Delta_{K+1}^\nu - \Delta_1^\nu + \Delta_K^\nu - \Delta_0^\nu \geq \hat{\mu}K \\ &\Leftrightarrow \Delta_{K+1}^\nu + \Delta_K^\nu \geq \Delta_0^\nu + \Delta_1^\nu + \hat{\mu}K, \end{aligned}$$

and since  $\Delta_{K+1} \leq \Delta_K$  (being  $\{\Delta_k\}_{k \in \mathbb{N}}$  monotone non-increasing), we finally obtain

$$\Delta_{K+1}^\nu \geq \frac{1}{2}(\Delta_0^\nu + \Delta_1^\nu + \hat{\mu}K),$$

from which we conclude that there exists a constant  $C > 0$  such that

$$\Delta_{K+1} \leq CK^{-\frac{1}{2\theta-1}}, \quad \forall K \in \mathbb{N},$$

and item (i) follows.

**Case  $\theta \in (0, \frac{1}{2})$ .** Since in this case  $2\theta \leq 1$  and  $\lim_{k \rightarrow \infty} \Delta_k = 0$ , we have  $\Delta_{k+1} \leq \Delta_{k+1}^{2\theta}$  for all sufficiently large  $k \in \mathbb{N}$ , and from (77) we get  $\Delta_{k+1} \leq \tilde{c}(\Delta_{k-1} - \Delta_{k+1})$ , or equivalently

$$\Delta_{k+1} \leq \left( \frac{\tilde{c}}{1 + \tilde{c}} \right) \Delta_{k-1}.$$

If  $k$  is odd, the iterative application of the previous inequality entails

$$\Delta_{k+1} \leq \left( \frac{\tilde{c}}{1 + \tilde{c}} \right)^{\frac{k+1}{2}} \Delta_0.$$

If  $k$  is even, the same reasoning leads to

$$\Delta_{k+1} \leq \left( \frac{\tilde{c}}{1 + \tilde{c}} \right)^{\frac{k}{2}} \Delta_1.$$

Therefore, for all  $k \in \mathbb{N}$ , we have

$$\Delta_{k+1} \leq C \left( \frac{\tilde{c}}{1 + \tilde{c}} \right)^{\frac{k}{2}}, \quad C = \max \left\{ \Delta_0 \sqrt{\frac{\tilde{c}}{1 + \tilde{c}}}, \Delta_1 \right\},$$

and the proof of item (ii) is complete.

## B Computation of the proximal operator of a least squares functional

Given the data fidelity term  $\mathcal{D}(x) = \frac{1}{2}\|Ax - b\|^2$ , where  $A \in \mathbb{R}^{n \times n}$  and  $x, y \in \mathbb{R}^n$ , we recall the closed-form expression of  $\text{prox}_{\alpha\mathcal{D}}(z)$ , with  $z \in \mathbb{R}^n$ , in the case where  $A$  represents either a blurring or a super-resolution operator.

If  $A = H$  is a convolution operator with circular boundary condition, it can be expressed as  $H = F^* \Lambda F$ , where  $F$  denotes the orthogonal discrete Fourier transform matrix,  $F^*$  its inverse, and  $\Lambda$

is diagonal. As a consequence, the computation of the corresponding proximal operator reduces to an element-wise inversion in the Fourier domain:

$$\text{prox}_{\alpha\mathcal{D}}(z) = F^* (I_n + \alpha\Lambda^*\Lambda)^{-1} F (\alpha H^T b + z).$$

If  $A = SH$  where  $S$  is the standard  $s$ -fold downsampling matrix of size  $m \times n$  and  $n = s^2 \times m$ , and  $H \in \mathbb{R}^{n \times n}$  is a convolution operator with circular boundary condition, then, in [50], the authors provide the closed-form computation of the proximal map for the data-fidelity  $\mathcal{D}(x)$ :

$$\text{prox}_{\alpha\mathcal{D}}(z) = \hat{z}_\alpha - \frac{1}{s^2} F^* \underline{\Lambda}^* \left( I_m + \frac{\alpha}{s^2} \underline{\Lambda} \underline{\Lambda}^* \right)^{-1} \underline{\Lambda} F \hat{z}_\alpha,$$

where  $\hat{z}_\alpha = \alpha H^T S^T b + z$  and  $\underline{\Lambda} = [\Lambda_1, \dots, \Lambda_{s^2}] \in \mathbb{R}^{m \times n}$ , with  $\Lambda = \text{diag}(\Lambda_1, \dots, \Lambda_{s^2})$  a blockdiagonal decomposition according to a  $s \times s$  paving of the Fourier domain. We remark that  $I_m + \frac{\alpha}{s^2} \underline{\Lambda} \underline{\Lambda}^*$  is a  $m \times m$  diagonal matrix and its inverse is computed element-wise.

## C Inexact computation of the proximal operator of a least squares functional restricted to a block of coordinates

To obtain a point  $\tilde{y}_k$  as defined in STEP 3 of Algorithm 1 when  $\phi(x) = \frac{1}{2} \|Ax - b\|^2$  and  $N \geq 1$ , we first make the following remark. Hereafter, we drop the iteration index  $k$  for simplicity.

*Remark.* Given  $x \in \mathbb{R}^n$ ,  $i \in \{1, \dots, N\}$  and  $U_j \in \mathbb{R}^{n \times n_j}$ ,  $j = 1, \dots, N$ , note that, in general,

$$\phi_i^x(z) = \phi \begin{pmatrix} U_1^T x \\ \vdots \\ U_{i-1}^T x \\ z \\ U_{i+1}^T x \\ \vdots \\ U_N^T x \end{pmatrix}.$$

Furthermore, if  $\phi(x) = \frac{1}{2} \|Ax - b\|^2$ , then

$$\begin{aligned} \phi_i^x(z) &= \frac{1}{2} \left\| A \left( (U_1^T x)^T, \dots, (U_{i-1}^T x)^T, z, (U_{i+1}^T x)^T, \dots, (U_N^T x)^T \right)^T - b \right\|^2 \\ &= \frac{1}{2} \left\| AU_i z - b + A \left( (U_1^T x)^T, \dots, (U_{i-1}^T x)^T, 0, (U_{i+1}^T x)^T, \dots, (U_N^T x)^T \right)^T \right\|^2 \\ &= \frac{1}{2} \|AU_i z - b_i^x\|^2, \end{aligned}$$

where  $b_i^x = b - A \left( (U_1^T x)^T, \dots, (U_{i-1}^T x)^T, 0, (U_{i+1}^T x)^T, \dots, (U_N^T x)^T \right)^T$ .

In view of this remark, we are interested in the inexact computation of the following proximal point

$$\text{prox}_{\alpha\phi_i^x}(\bar{x}_i) = \underset{y \in \mathbb{R}^{n_i}}{\text{argmin}} \phi_i(y) + \frac{1}{2\alpha} \|y - \bar{x}_i\|^2, \quad (96)$$

where  $\bar{x}_i = U_i^T(x + \beta(x - w)) - \alpha U_i^T \nabla f(x)$ , being  $x, w \in \mathbb{R}^n$ ,  $\alpha, \beta \in \mathbb{R}^+$ , and  $\phi_i : \mathbb{R}^n \rightarrow \mathbb{R}$  is the least squares function given by

$$\phi_i^x(y) = \frac{1}{2} \|AU_i y - b_i^x\|^2. \quad (97)$$

The following procedure is an application of the more general framework discussed in [13, Appendix A] for computing inexact proximal points satisfying condition (25). Let us rewrite function (97) as

$$\phi_i^x(y) = \omega_x(M_i y),$$

with  $\omega_x : \mathbb{R}^n \rightarrow \mathbb{R}$ ,  $\omega_x(\cdot) = \frac{1}{2} \|\cdot - b_i^x\|^2$ , and  $M_i = AU_i \in \mathbb{R}^{n \times n_i}$ . Note that  $\omega_x(t) = \rho(t - b_i^x)$ , where  $\rho(\cdot) = \frac{1}{2} \|\cdot\|^2$ . By using a well-known calculus rule holding for conjugate functions [27, Proposition 1.3.1(v)], we conclude that

$$\omega_x^* : \mathbb{R}^n \rightarrow \mathbb{R}, \quad \omega_x^*(s) = \rho^*(s) + s^T b_i^x = \frac{1}{2} \|s\|^2 + s^T b_i^x.$$

The primal problem associated to the computation of (96) writes as

$$\begin{aligned} \min_{y \in \mathbb{R}^{n_i}} h(y) &\equiv \phi_i^x(y) - \phi_i^x(U_i^T x) + \frac{1}{2\alpha} \|y - U_i^T x\|^2 + \langle U_i^T \nabla f(x) - \frac{\beta}{\alpha} U_i^T(x - w), y - U_i^T x \rangle \\ &= \omega_x(M_i y) + \frac{1}{2\alpha} \|y - \bar{x}_i\|^2 - \phi_i^x(U_i^T x) - \frac{\alpha}{2} \left\| U_i^T \nabla f(x) - \frac{\beta}{\alpha} U_i^T(x - w) \right\|^2. \end{aligned} \quad (98)$$

Note that the primal function  $h$  has the same form as the function  $h_k$  defined at each iteration of Algorithm 1. On the other hand, by means of (98), we can write the dual problem as follows

$$\begin{aligned} \max_{v \in \mathbb{R}^n} \psi(v) &\equiv -\omega_x^*(v) - \frac{1}{2\alpha} \|\bar{x}_i - \alpha M_i^* v\|^2 + \frac{1}{2\alpha} \|\bar{x}_i\|^2 - \phi_i(U_i^T x) - \frac{\alpha}{2} \left\| U_i^T \nabla f(x) - \frac{\beta}{\alpha} U_i^T(x - w) \right\|^2 \\ &= -\frac{1}{2} \|v\|^2 - v^T b_i^x - \frac{1}{2\alpha} \|\bar{x}_i - \alpha U_i^T A^T v\|^2 + \underbrace{\frac{1}{2\alpha} \|\bar{x}_i\|^2 - \phi_i(U_i^T x) - \frac{\alpha}{2} \left\| U_i^T \nabla f(x) - \frac{\beta}{\alpha} U_i^T(x - w) \right\|^2}_{=constant}. \end{aligned} \quad (99)$$

By definition of the Fenchel dual, we have

$$h(y) \geq \psi(v), \quad \forall y \in \mathbb{R}^{n_i}, \forall v \in \mathbb{R}^n.$$

In particular, the previous inequality holds for  $y = \hat{y} = \text{prox}_{\alpha\phi_i^x}(\bar{x}_i)$  and for any  $v \in \mathbb{R}^n$ . Therefore if  $(\hat{y}, v)$  is a primal dual pair satisfying

$$h(\hat{y}) \leq \frac{2}{2 + \tau} \psi(v),$$

then  $\hat{y}$  is an inexact proximal gradient point in the sense of (25). According to [13, Proposition 19], the existence of such a pair is guaranteed, and it can be computed in practice. For completeness, we restate the proposition in the context of our framework.

*Proposition C.1.* Given  $\phi_i^x$  defined as is (97), let  $\{v_\ell\}_{\ell \in \mathbb{N}} \subset \mathbb{R}^n$  be a sequence such that

$$\lim_{\ell \rightarrow +\infty} v_\ell = \operatorname{argmax}_{v \in \mathbb{R}^n} \psi(v).$$

By defining the corresponding primal sequence  $\{\tilde{y}_\ell\}_{\ell \in \mathbb{N}} \subset \mathbb{R}^{n_i}$  as

$$\tilde{y}_\ell = \bar{x}_i - \alpha M_i^* v_\ell = \bar{x}_i - \alpha U_i^T A^T v_\ell, \quad \forall \ell \in \mathbb{N},$$

it holds that

$$\lim_{\ell \rightarrow +\infty} \psi(v_\ell) = \lim_{\ell \rightarrow +\infty} h(\tilde{y}_\ell) = h(\text{prox}_{\alpha\phi_i^x}(\bar{x}_i)).$$

Therefore the inequality

$$h(\tilde{y}_\ell) \leq \frac{2}{2 + \tau} \psi(v_\ell)$$

holds for all sufficiently large  $\ell$ , for any given  $\tau > 0$ .

The dual sequence  $\{v_\ell\}_{\ell \in \mathbb{N}}$  can be obtained by applying an iterative gradient-based optimization scheme to the dual problem, which is stopped at the first iteration  $\ell^*$  satisfying

$$h(\tilde{y}_{\ell^*}) \leq \frac{2}{2 + \tau} \psi(v_{\ell^*}).$$

According to Proposition C.1,  $\tilde{y}$  can be fixed as  $\tilde{y}_{\ell^*}$ .

The solution of the dual problem (99) can be derived by means of the optimality condition

$$-v - b_i^x - (-AU_i \bar{x}_i + \alpha A^T U_i U_i^T A^T v) = 0 \quad (100)$$

$$(I + \alpha AU_i U_i^T A^T) v = AU_i \bar{x}_i - b_i^x, \quad (101)$$

and it can be computed iteratively by using a variant of the Gauss-Seidel method, observing that the matrix on the left can also be seen as

$$(I + \alpha AU_i U_i^T A^T) = (I + \alpha AA^T - \alpha AU_{iC} U_{iC}^T A^T). \quad (102)$$

So the iteration of the subroutine for the inexact computation of the restricted proximal operators reads as

$$v_{\ell+1} = (I + \alpha AA^T)^{-1} (A^T U_i \bar{x}_i - b_i^x + \alpha AU_{iC} U_{iC}^T A^T v_\ell), \quad (103)$$

where the inverse is computed in closed form, similarly to B and  $U_{iC} U_{iC}^T = I - \tilde{U}_i$ .